Chapter 29

Machine Learning for Cerebrovascular Disorders

Yannan Yu and David Yen-Ting Chen

Abstract

Cerebrovascular disease refers to a group of conditions that affect blood flow and the blood vessels in the brain. It is one of the leading causes of mortality and disability worldwide, imposing a significant socioeconomic burden to society. Research on cerebrovascular diseases has been rapidly progressing leading to improvement in the diagnosis and management of patients nowadays. Machine learning holds many promises for further improving clinical care of these disorders. In this chapter, we will briefly introduce general information regarding cerebrovascular disorders and summarize some of the most promising fields in which machine learning shall be valuable to improve research and patient care. More specifically, we will cover the following cerebrovascular disorders: stroke (both ischemic and hemorrhagic), cerebral microbleeds, cerebral vascular malformations, intracranial aneurysms, and cerebral small vessel disease (white matter hyperintensities, lacunes, perivascular spaces).

Key words Cerebrovascular disorders, Machine learning, Stroke, Cerebral microbleeds, Cerebral vascular malformations, Intracranial aneurysms, Cerebral small vessel disease, White matter hyperintensities, Lacunes, Perivascular spaces

1 Introduction

Cerebrovascular disorders are a group of conditions that affect blood vessels in the brain and cerebral blood circulation. Stroke is the most common presentation of cerebrovascular disorders. The majority of strokes are ischemic, caused by decreased blood flow to the brain leading to damage of brain tissue and neurologic dysfunction. Less common are hemorrhagic strokes, caused by blood extravasation out of cerebral blood vessels into the brain tissue itself (intracranial hemorrhage) or in spaces surrounding brain tissue (subarachnoid and subdural hemorrhage). Hemorrhagic strokes can lead to catastrophic injury due to increased intracranial pressure, decreased brain tissue perfusion, and damaged normal brain tissue. In 2019, there were 6.6 million deaths attributable to cerebrovascular disease worldwide; three million individuals died of ischemic stroke, 2.9 million died of intracerebral hemorrhage, and 0.4 million died of subarachnoid hemorrhage [1]. Stroke is the

second leading cause of death, accounting for 11.6% of all deaths globally, and the third leading cause of death and disability combined, contributing to 143 million disability-adjusted life years [2]. Cerebral small vessel disease encompasses a spectrum of disorders affecting the brain's small perforating arterioles, capillaries, and venules. It has a wide range of clinical manifestations, causing approximately 25% of strokes and contributing to approximately 45% of dementia cases [3]. Cerebral small vessel disease is highly prevalent in the elderly population, affecting from 5% of people at age 50 to almost 100% of people older than 90 years [3]. Intracranial aneurysms (IA) are due to ballooning in a blood vessel in the brain; if aneurysms rupture, they can lead to catastrophic subarachnoid hemorrhage with a mortality rate of 23–51% [4, 5] and permanent disability in 30–40% [4, 6]. Arteriovenous malformations (AVM) are due to a tangle of blood vessels in the brain that bypass normal brain tissue; AVMs can cause hemorrhage and seizures.

Cerebrovascular disorders are commonly diagnosed with imaging studies, and the treatment of some cerebrovascular disorders is based on imaging guidance. Common imaging modalities include computed tomography (CT), magnetic resonance imaging (MRI), and digital subtraction angiography (DSA). CT provides a rapid exam of brain tissue and brain vessels; some of the CT protocols will be mentioned in this chapter including non-contrast CT, CT angiography (CTA), and CT perfusion (CTP). Non-contrast CT is the exam of choice for diagnosing intracranial hemorrhage and also the exam of choice for initial triaging of ischemic stroke. However, ischemic stroke presentation on non-contrast CT depends mostly on stroke age, ranging from no change or subtle changes in 0–6 h to obvious hypoattenuation after 24 h. Post-contrast CT, depending on the detailed protocol, can highlight the vascular structures known as CTA often used in diagnose artery occlusion in ischemic stroke, IA, or AVM. Post-contrast CT can also calculate brain blood perfusion status known as CTP, commonly used in ischemic stroke triaging. MRI has various sequences that give tissue a particular appearance for medical diagnosis. Some of the sequences that will be mentioned in this chapter include the following. Diffusion-weighted imaging (DWI) measures water molecule movement restriction and is very sensitive to injured tissue in stroke. Perfusion-weighted imaging (PWI) and arterial spin labeling (ASL) both measure brain perfusion, but PWI requires contrast injection, while ASL does not. They are often used in ischemic stroke. Gradient-recalled echo (GRE) and susceptibility-weighted images (SWI) are both sensitive to iron and calcium deposition and used in blood product detection and can be used for detecting hemorrhage and small vessel disease. T2-weighted fluid-attenuated inversion recovery (FLAIR) is commonly used to detect stroke lesions >6 h and small vessel disease. For CT perfusion and MR

perfusion, quantitative perfusion maps can be calculated to estimate the blood perfusion status, common ones including cerebral blood flow (CBF), cerebral blood volume (CBV), time-to-maximum of residue function (Tmax), and mean transit time (MTT). DSA is a fluoroscopic technique (similar to X-ray) to visualize vasculature, which is used for the diagnosis and treatment of IA, ischemic stroke artery occlusions, and some AVMs.

Machine learning holds the promise of optimizing cerebrovascular disorder care, with the potential ability to improve or accelerate diagnosis and provide prognostication utilizing both clinical and imaging data.

2   Ischemic Stroke

Approximately 87% strokes are ischemic and 13% are hemorrhagic [1]. Ischemic stroke is due to reduced or absent blood supply to part of the brain, typically due to an occlusion or stenosis of a cerebral artery, leading to localized brain tissue damage and loss of neurological function. Ischemic damage to the brain is strongly time-dependent [7]. The only recommended treatments available to treat or mitigate damage due to ischemic stroke are IV thrombolysis within 4.5 h of symptom onset and endovascular thrombectomy within 24 h of symptom onset; these treatments are only approved for specific subsets of stroke patients [8]. Acute stroke therapies work to recanalize an occluded cerebral blood vessel and restore blood flow to ischemic or hypoperfused brain tissue, specifically via intravenous medication that can break up the occlusion (thrombolysis) or mechanical removal of the occlusion within the culprit artery (endovascular thrombectomy). Because clinical protocols are time-sensitive and standardized, timely diagnosis of ischemic stroke and rapid initiation of treatment are crucial steps in clinical practice [7]. Therefore, there is great potential for machine learning-based algorithms in acute ischemic stroke care. Figure 1 is a general example of how stroke is typically diagnosed and treated in the clinical setting.

In this section, we review studies that investigated machine learning application in large vessel occlusion (LVO) diagnosis, stroke onset time evaluation, stroke lesion segmentation, stroke outcome, and complication prediction. Common imaging modalities in acute stroke were computed tomography (CT) and magnetic resonance imaging (MRI) for stroke diagnosis and triaging and digital subtraction angiography (DSA) for both stroke diagnosis and treatment. Examples of those imaging modalities are demonstrated in Figs. 2 and 3.
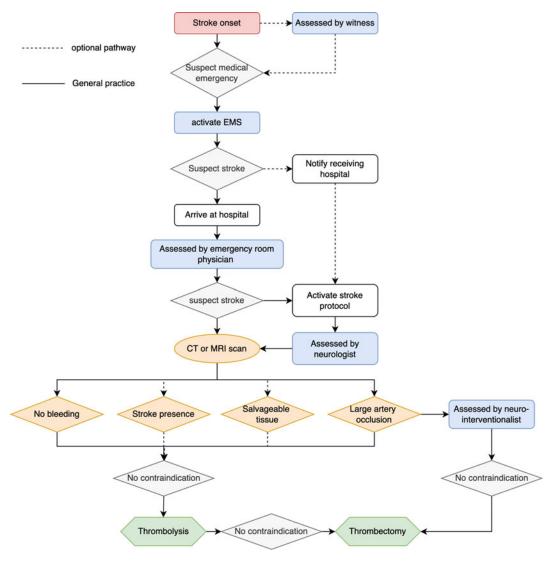
Fig. 1 General pathway of stroke diagnosis and treatment. Solid line represents general practice; dashed line represents optional pathway. EMS emergency medical service, CT computed tomography, MRI magnetic resonance imaging

2.1 Diagnosing Large Vessel Occlusion (LVO)

Large vessel occlusions are defined as blockages of the proximal intracranial arteries, accounting for approximately 24–46% of acute ischemic strokes [9]. Diagnosing an LVO is an important step of stroke diagnosis and treatment considerations; patients with LVO are potential candidates for endovascular thrombectomy, which is the most effective treatment available to recanalize an occluded artery [8, 10, 11]. Endovascular thrombectomy is a highly specialized procedure, and the personnel and equipment needed for thrombectomy are not widely available. Patients often need to be transferred from the hospital where they are initially evaluated to
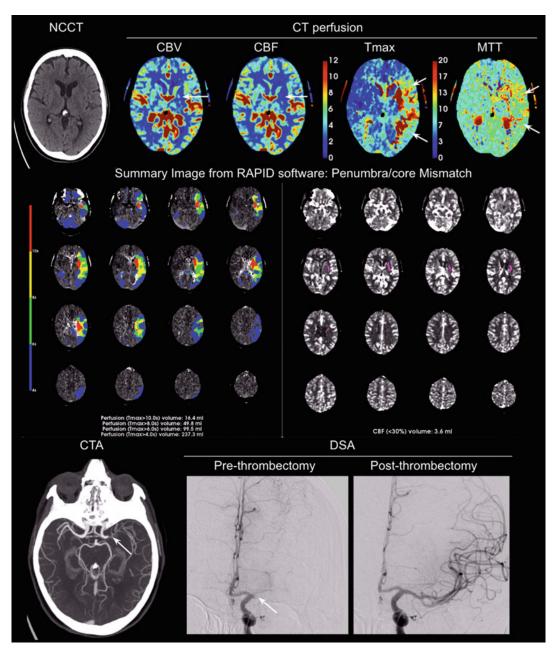
Fig. 2 Common CT scans used in acute stroke. This example case showed left-sided stroke (on the right side of the image) with occlusion of the middle cerebral artery (M1 segment). The NCCT had only very subtle changes, and the CT perfusion showed large perfusion deficit (asymmetrically low measures in CBF and asymmetrically high measures on Tmax and MTT) and small irreversible tissue injury. Penumbra/core mismatch is the volume ratio between prolonged Tmax area and decreased CBF area; the summary image from RAPID software showed mismatch ratio of 99.5 mL/3.6 mL. CTA showed middle cerebral artery main trunk (M1 segment) occlusion. The DSA image showed recanalization of the artery occlusion after thrombectomy. NCCT non-contrast computed tomography, CBV cerebral blood volume, CBF cerebral blood flow, Tmax time to maximum of the tissue residue function, MTT mean transit time, CTA computed tomography angiography, DSA digital subtraction angiography
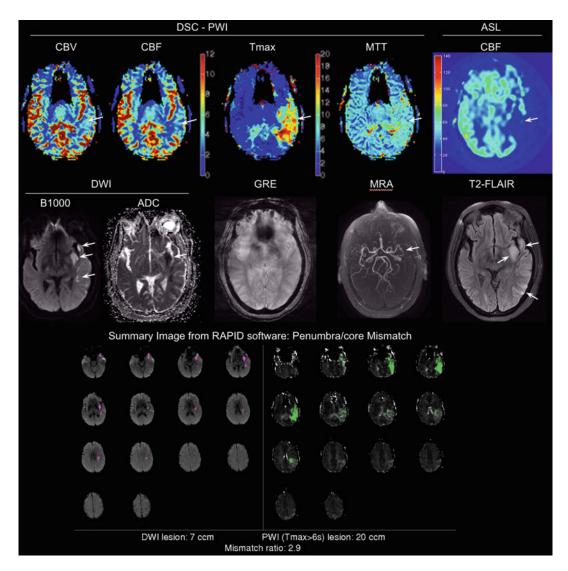
Fig. 3 Common MRI sequences used in acute stroke. This example case showed left-sided stroke (on the right side of the image) with occlusion of a middle cerebral artery branch (M2 segment, inferior division). The DSC-PWI and ASL showed the perfusion deficit (asymmetrically low measures in CBF and asymmetrically high measures on Tmax and MTT), which was much greater than the irreversible tissue injury on DWI, with a mismatch ratio of 2.9. GRE did not show blooming effect (a common finding of acute intra-arterial thrombus), MRA showed a left-sided large vessel occlusion (M2 segment, white arrow), and T2-FLAIR taken 24 h after the stroke showed injured brain tissue after the stroke (white arrows). DSC-PWI dynamic susceptibility contrast perfusion-weighted imaging. ASL arterial spin labeling, CBV cerebral blood volume, CBF cerebral blood flow, Tmax: time to maximum of the tissue residue function, MTT mean transit time, DWI diffusion-weighted imaging, ADC apparent diffusion coefficient, GRE gradient-recalled echo sequence, MRA magnetic resonance angiography, T2-FLAIR T2-weighted fluid-attenuated inversion recovery

a comprehensive stroke center with specialists who perform thrombectomy. Non-specialized hospitals must have the ability to reach the initial diagnosis of LVO-related stroke and arrange urgent

transfer to a comprehensive stroke center. During initial triage, automatic detection of LVO may accelerate the acute stroke protocol and patient transfer [12].

CT angiography (CTA) is the image modality of choice for rapid, non-invasive diagnosis of a large vessel occlusion. Several studies have used machine learning to demonstrate the feasibility to identify LVO on CTA. Viz.ai developed a commercial method of LVO detection that was achieved by a two-step analysis of CTA vessel segmentation via a 3D U-Net and large vessel classification via comparison of endpoint length and Hounsfield unit (a standardized unit for CT image pixel) value in MCA branch segmentation. Yahav-Dovrat et al. [13] reported the performance of this system in a prospective cohort of 404 stroke protocol CTAs. Seventy-two of the 404 stroke protocol CTAs had an LVO, and the software showed a sensitivity of 82%, a positive predictive value of 64%, and a negative predictive value of 96%. The relatively low sensitivity and positive predictive value may limit the clinical utility of the reported model, as the screening process of acute ischemic stroke requires high sensitivity. Stib et al. [14] trained convolutional neural networks (CNNs) with maximal intensity projection (MIP) images of multiphase CTA from 270 patients with LVO and 270 without LVO. The authors then tested the model in a balanced dataset of 62 patients, which showed a sensitivity of 100% and specificity of 77% by using all phases in multi-phase CTA, exceeding the performance of single-phase CTA with a sensitivity of 77% and specificity of 71%. To note, a non-deep learning-based commercial method from RAPID showed excellent sensitivity and specificity (above 95%) in an independent validation cohort [15]. These automated technologies have already become integrated into the clinical practice of many stroke systems of care, and further refinement of algorithm for center-specific population may improve the clinical performance.

LVO can also be detected from non-angiographic images, specifically non-contrast CT, which is more widely available than CTA. CTA requires intravenous contrast injection, which is typically not given to patients with kidney failure and/or an allergy to iodinated contrast. You et al. [16, 17] reported a XGBoost model trained with 200 cases' clinical data and non-contrast CT image features extracted from the bottleneck of U-Net; the model showed a sensitivity of 95.3% and specificity of 68.4% in 100 test cases. Olive-Gadea et al. [18] reported a DenseNet and decision tree-based prediction model to diagnose LVO from non-contrast CT images, showing a sensitivity of 83.1% and specificity of 85.1%, which exceeded the performance of a National Institutes of Health (NIH) stroke scale-based model.

Digital subtracted angiography (DSA) is an invasive diagnostic method for LVO used to guide interventional neuroradiologists treating the vascular occlusion. Thrombectomy treatment is

performed under the guidance of DSA to retrieve the thrombus causing occlusion. However, reading DSA images requires highly specialized training in interventional neuroradiology, and a real-time evaluation of treatment effect during the thrombectomy procedure is often required. Thrombolysis in cerebral infarction (TICI) scale is an evaluation on DSA for stroke treatment effect after thrombectomy procedure. Previous studies reported that the inter-reader agreement of TICI was low [19, 20]. Machine learning on DSA studies is challenging because the DSA contains 2D projection images from a 3D vasculature which are sensitive to the position of the X-ray detector plane, as well as temporal information that makes the data more similar to a video. When reading the DSA images, radiologists focus on the anatomical difference compared to the normal atlas, the speed of contrast filling into the arteries, the extent of contrast filling into the capillary system, and the contrast drainage from the veins.

Ueda et al. [21] collected DSA images with and without misregistration artifact and applied U-Net and convolutional patch generative adversarial network architecture as generator and discriminator networks to predict non-misregistered DSA from misregistered DSA. Zhang et al. [22] proposed a U-Net to track and segment the brain vessels from DSA, which could be the first step for building a diagnostic tool. As DSA is a 2D image with temporal information, studies used different strategies to blend these features into a neural network. Bhurwani et al. [23] proposed an ensembled convolutional neural network for post-thrombectomy DSA images and predict the reperfusion status. They achieved a sensitivity of 90% and specificity of 74% on diagnosing reperfusion after thrombectomy. Su et al. [24] proposed a curated algorithm including phase classification, motion correction, and perfusion segmentation to achieve final TICI scoring using ResNet-18. They achieved an agreement of 90% between the algorithm and human reader. To note, human-to-human agreement was 89%. Researchers from the same group [25] also designed a sophisticated network for spatial and temporal feature extraction and predict perforation, a complication from thrombectomy procedure. The model predicted perforation with precision of 0.83 and recall of 0.70, a performance similar to that of human expert readers.

In addition to classifying LVO on imaging, studies also showed it is feasible to predict LVO based on clinical evaluation, which could prepare the emergency medical services (EMS) for direct transport to comprehensive stroke centers [26–30]. Chen et al. [27] trained ANN models using tenfold cross-validation on 600 patients with 1:1 ratio of LVO and non-LVO using patients' NIHSS breakdown score, demographics, medical history, and risk factors as input. The ANN models reached sensitivity of 0.807 and specificity of 0.833. Wang et al. [26] from the same group then trained 8 machine learning models on 15,365 patients and test on

4215 patients using their NIHSS, demographics, medical history, and risk factors as input. They showed random forest model performed the best with an AUC of 0.831, sensitivity of 0.721, and specificity of 0.827.

2.2 Predicting Stroke Onset Time

In 14–27% of strokes, the symptom onset time is not known [31–33]. For those patients, identifying the likely onset time is crucial for proper treatment. Indeed, it is key to know if one is still within the treatment window for intravenous thrombolysis (within 4.5 h) or endovascular therapy (within 6 h if presence of LVO plus no extensive lesion on non-contrast CT or 24 h if presence of LVO and target mismatch on perfusion imaging). MRI plays a key role in estimating the duration of stroke. Studies have shown that fluid-attenuated inversion recovery (FLAIR) usually detects ischemic lesion after 3–6 h of stroke onset [34, 35], in contrast to diffusion-weighted imaging (DWI), which detects ischemic lesions within minutes of stroke. Therefore, the "mismatch" between FLAIR and DWI may be used as a clock for determining stroke onset time [36]. Lee et al. [37] captured 89 vector features from DWI and FLAIR imaging and trained machine learning models including logistic regression, support vector machine, and random forest to classify if the stroke onset is within 4.5 h. They found the machine learning models were more sensitive (75.8% vs 48.5%, $p = 0.01$) but less specific (82.6% vs 91.3%, $p = 0.15$) compared to human readers. Similar results were also achieved by other research groups [38]. Perfusion MRI has not been studied in the past for determining the stroke onset time. Ho et al. [39, 40] extracted deep features using an autoencoder from perfusion MRI to classify whether stroke onset time was within 4.5 h (the current time window for intravenous tissue plasminogen activator [tPA]). Using input DWI, apparent diffusion coefficient (ADC), FLAIR, and perfusion-weighted images, they achieved a ROC AUC of 0.765. This approach outperformed DWI-FLAIR-based machine learning methods (AUC of 0.669) and clinical methods (AUC of 0.58) in the same dataset. The use of imaging to determine the time of stroke onset may increase the number of patients eligible for time-limited stroke treatments, such as intravenous thrombolysis [31].

2.3 Stroke Lesion Segmentation

Non-contrast-enhanced CT scan is the most common initial imaging obtained for stroke patients. Therefore, CT datasets are usually much more common and larger than MRI datasets. However, it is generally more challenging to diagnose early stroke or predict final stroke lesions on CT than MRI, as changes on CT related to early hyperacute phase (<6 h) of ischemic stroke are very subtle, including loss of gray and white matter differentiation, hypoattenuation of deep nuclei, and cortical hypodensity with associated parenchymal swelling and gyral effacement. The Alberta Stroke Program

Early CT Score (ASPECTS) is a scoring system that assesses stroke lesion presence based on early hyperacute phase changes on non-contrast CT image; scores range from 0 to 10, with 0 representing extensive ischemic damage and 10 representing no evidence of ischemia [41]. Current guidelines recommend reperfusion treatment for those with high ASPECTS [8], meaning less injured tissue, but ongoing research and trials are investigating the benefit of treating low ASPECTS stroke patients [42]. DWI/ADC is the most common and accurate MRI sequence to identify early stroke lesions (using a threshold of ADC $\leq 620 \times 10^{-6}$ mm^2/s). In addition, automated segmentation on MRI/CT would benefit acute treatment decisions as well as enable researchers to conduct clinical research on a much larger scale.

Many studies have showed the use of machine learning for stroke lesion segmentation on acute to subacute CTs and MRIs [43–57]. Kuang et al. [58] trained a random forest classifier on non-contrast CT images from 157 stroke patients to predict the ASPECTS score on MRI scanned within 1 h after the CT image and tested on 100 patients. They achieved a sensitivity of 66.2% and specificity of 91.8% in 100 × 10 ASPECTS regions and sensitivity of 97.8% and specificity of 80% in classifying ASPECT >4 and ≤4. Qiu et al. [57] from the same group used the same dataset to segment the early stroke lesion on non-contrast CT images using MRI as ground truth. They proposed a random forest algorithm with sophisticated feature engineering of distance feature, atlas encoded lesion location feature, and U-Net generated probability map of lesions from a separate dataset as input. They showed good correlation between predicted stroke lesion volume and ground truth ($r = 0.76$) and mean volume difference of 11 mL. Two commercial software programs for automatic ASPECTS scoring (e-ASPECTS, Brainomix, and Rapid ASPECTS, iSchemaView) are available and reported to be not inferior or even more accurate than clinicians [59–64].

The Ischemic Stroke Lesion Segmentation (ISLES) 2015 challenge provided training and testing data for subacute stroke lesion segmentation using MRI sequences including DWI and FLAIR. In this challenge, the highest performance for lesion segmentation was achieved by a 3D CNN with Dice score coefficient (DSC) of 0.57 [45]. Chen et al. [43] developed a two-step method to segment stroke lesions from DWI, reaching a DSC of 0.67. The first step was using an encoder-decoder CNN to propose a lesion segmentation, with a second step CNN which took patches of original DW images and previous output at multiple scales as input and classified the proposed segmentation as true or false. Other studies reached similar results (DSC 0.64–0.76) with 2D and 3D encoder-decoder CNNs [47–50]. The ISLES 2018 challenge provided training and testing data for acute stroke CT perfusion imaging to predict irreversibly injured tissue defined on DWI [65]. The top team

used a 3D multi-scale U-Net with atrous convolution algorithm and achieved an average DSC and an average absolute volume difference of 0.51 and 10.2 mL, respectively [66]. Other studies also reached similar results but were less accurate than the top performing team (DSC 0.44–0.49) [67, 68].

The aforementioned methods require manual labeling of stroke lesions on many images to serve as training, which is expensive and limits the scale of medical image deep learning research. For this reason, Zhao et al. [52] explored semi-supervised algorithms (a combination of K-means clustering and CNN) in a weakly labeled stroke segmentation dataset using acute DWI and ADC, reaching a mean DSC of 0.64. Federau et al. [53] explored 3D U-Net segmentation using a dataset augmented with synthetic stroke lesions on DWI, achieving a DSC of 0.72. More recently, Zhang et al. [51] utilized a feature pyramidal network [69] and a U-Net with multi-plane (axial, sagittal, and coronal planes) DWI to perform lesion segmentation, which achieved a DSC of 0.62. As radiologists usually interpret MRI by looking at different sequences, neural networks that take different imaging sequences as input and "fuse" their information are an important research direction to improve the diagnosis.

Winzeck et al. [55] proposed to train an ensemble of CNNs instead of individual CNNs. The authors adopted the CNN structure from the highest performance model in ISLES 2015 challenge. They found that an ensemble of five 3D CNNs segmented the DWI lesion from ADC, DWI, and B0 images more accurately than individual CNNs (median DSC 0.82 vs 0.79). Wu et al. [44], from the same group, trained the ensemble of CNNs with a multi-center, multi-vendor dataset with ADC, DWI, and B0 data and found that it performed better than models trained with a single-center dataset, with a median DSC of 0.86 (IQR 0.79–0.89). Although the model performance cannot be directly compared between papers as they all used different test datasets, this chapter has reported the highest DSC in stroke lesion segmentation so far.

2.4 Predicting Stroke Lesions in the Future

As compared to the stroke lesion segmentation on a single-time point imaging, segmenting a final lesion or hemorrhagic transformation on follow-up images using baseline CT/MRI is a way to predict patient clinical and radiographic outcome in the future. In particular, methods that can predict individual response to treatment (e.g., predicting the future outcomes in the presence and absence of treatment) can be useful to determine whether the treatment would benefit to this individual.

The ISLES challenges from 2016 and 2017 were focused on stroke lesion prediction from initial MRIs, including diffusion and perfusion imaging [70]. Compared to human inter-reader agreement of DSC of 0.58, the best performing model, using an

encoder-decoder CNN, achieved a DSC of 0.32 [70]. Using data from this challenge, Pinto et al. [71] proposed an encoder-decoder CNN combined with 2D gated recurrent unit layers [72], with the TICI score fused at the end to generate lesion predictions based on different TICI scores. The model had a similar DSC of 0.35. Nielsen et al. [73] used a CNN to predict the final stroke lesion using baseline DWI and MR perfusion and reported an ROC AUC of 0.88. They also found CNNs trained with either treatment or no treatment predicted different stroke lesions, suggesting a role to use such models to explore differential outcomes with therapy. Ho et al. [74] proposed a CNN model to predict lesions directly from PWI source images (i.e., rather than from the parameter maps created by post-processing software), which reached a similar ROC AUC of 0.871. Yu et al. [75] showed that an attention-gated U-Net model could predict final stroke lesions at 2–7 days from baseline MR perfusion and diffusion images regardless of reperfusion status with a median DSC of 0.53 and ROC AUC of 0.92. In a separate study aimed at providing more accurate penumbra and ischemic core information, Yu et al. [76] pre-trained an attention-gated U-Net model with DWI and MR perfusion maps in patients with partial reperfusion or unknown reperfusion and then fine-tuned this pre-trained model with minimal reperfusers to predict penumbra and major reperfusers to predict ischemic core. The model achieved a median DSC of 0.60 for penumbra and 0.57 for ischemic core, exceeding the performance of the automated penumbra and ischemic core segmentation from state-of-the-art software. In a slightly different approach, Wang et al. [77] used a CNN to identify penumbral tissue (as defined by the Tmax perfusion parameter from contrast PWI) on non-contrast arterial spin labeling (ASL) with an ROC AUC of 0.958 which provided similar stroke triaging in 92% of cases without the need to inject a contrast agent.

It is more challenging to predict the final stroke lesion from CT image as the markers are not correlated with tissue injury as well as DWI. Robben et al. [78] proposed a CNN with parallel inputs from source CT perfusion images and clinical metadata, which achieved a mean DSC of 0.48. An ablation study was also performed, which showed in addition to image information, time from imaging to treatment also influenced the model prediction. Amador et al. [79] applied temporal CNN to predict the final lesion from the baseline CT perfusion source image, which achieved a DSC of 0.33. Kuang et al. [80] trained a random forest model from 67 patients' CT perfusion maps and clinical data and tested in 137 patients. They found the model reached a median volumetric difference of −3.2 mL and DSC of 0.388 and the model was significantly more accurate than thresholding methods (Tmax thresholding and CBF thresholding), although the reperfusion status of those patients were heterogeneous.

2.5 Predict Hemorrhagic Transformation

Hemorrhagic transformation is a potential complication of stroke treatment. Large hemorrhagic transformation can be lethal. Predicting hemorrhagic transformation after reperfusion therapy has been investigated in the past using statistical methods. To improve the prediction, Yu et al. [81, 82] proposed a long short-term memory network (LSTM) to predict the segmentation of hemorrhagic transformation lesion identified by gradient-recalled echo (GRE) sequence performed at 24 h after stroke onset, using baseline MR perfusion as input. The model demonstrated an ROC AUC of 0.894, which was higher than a previous SVM approach (ROC AUC of 0.837). Jiang et al. [83] included multi-parametric MRI and clinical data to predict the presence of hemorrhagic transformation. The image sequences were separately fed in to inception V3 architecture and connected with clinical data at the fully connected layers. The model achieved a high AUC of 0.932 and an accuracy of 0.873 in binary classification of hemorrhagic transformation.

2.6 Predicting Stroke Clinical Outcomes

Compared to predicting future stroke lesions on images, clinical outcome prediction is more difficult for several reasons. The most common scoring system, the modified Rankin score (mRS), is nonlinear and subjective, and the unit of analysis is each patient rather than each voxel (Table 1). The majority of the previously published studies used non-imaging data as input to predict clinical outcomes using simple statistical or more complex machine learning models [84–89]. However, images may provide more information such as the spatial location of infarct and hemorrhage and the presence of brain atrophy. Osama et al. [90] proposed a parallel multi-parametric feature-embedded Siamese neural network [91] to classify 3-month mRS from 0 to 4 using the MRI perfusion maps and clinical data from the ISLES 2017 challenge. This model achieved an average accuracy of 37% on each class using leave-one-out cross-validation testing. Nishi et al. [92] proposed a U-Net with DWI as input and stroke lesion segmentation as output. Then the bottleneck features of the U-Net were extracted to predict whether the 3-month mRS would be greater than 2, a common metric of good clinical outcome. This method achieved a ROC AUC of 0.81, exceeding the performance of ASPECTS Score (ROC AUC of 0.63) and ischemic core volume models (ROC AUC of 0.64). These studies show promise that automated imaging analysis might be helpful in the prediction of clinical outcomes, but further study into these complex and ambitious predictions is needed.

Table 1
Modified Rankin scale

0	No symptoms at all
1	No significant disability despite symptoms; able to carry out all usual duties and activities
2	Slight disability; unable to carry out all previous activities, but able to look after own affairs without assistance
3	Moderate disability; requiring some help, but able to walk without assistance
4	Moderately severe disability; unable to walk without assistance and unable to attend to own bodily needs without assistance
5	Severe disability; bedridden, incontinent, and requiring constant nursing care and attention
6	Dead

2.7 Predicting Cerebral Blood Flow (CBF) and Cerebrovascular Reserve (CVR)

Sometimes, it is useful to obtain more accurate images of biomarkers that drive stroke severity, such as CBF. The current CBF gold standard, O-15 water positron emission tomography (PET), is much less accessible than MRI or CT given its strict requirement for radiotracer production within the facility and exposure to radiation. ASL, a non-invasive MRI sequence measuring CBF without the use of intravenous contrast, allows repeat examination and limits any potential adverse effects from contrast or radiotracer agent. Although ASL has been improved over the last decades, it has low sensitivity, frequently underestimates CBF in areas with delayed collateral flow, and is prone to a range of artifacts. Guo et al. investigated whether a U-Net CNN can produce PET-like CBF maps from ASL and structural images [93]. Compared to the ASL CBF, the synthetic PET CBF map derived from the ASL and structural MRI scans had a significantly higher structural similarity index (0.854 ± 0.036 vs 0.743 ± 0.045). By training on both normal subjects and patients with cerebrovascular disease, they showed similar good performance to predict a PET CBF map regardless of disease status.

CVR is measured by calculating relative CBF change ($r\Delta CBF$) before and after a vasodilating drug. Patients with low CVR are at higher risk of future stroke, and the identification of these patients may be helpful in the initiation of preventative treatments, such as aggressive medical therapy, carotid endarterectomy, or carotid stent placement [94]. Acetazolamide, a carbonic anhydride inhibitor, is typically used as a vasodilator to measure CVR. It is generally safe, but it is contraindicated in patients with sulfa allergies or severe kidney and liver diseases. Some patients may present with stroke-like symptoms during the test. These symptoms, although transient and rare, may unsettle patients and medical staff.

To further simplify the measurement of CVR, Chen et al. [95] investigated the feasibility of a drug-free CVR measurement using a

U-Net CNN based on the work of Guo et al. [93]. The study also investigated several input combinations (MRI + PET vs MRI only) to determine whether baseline O-15 PET CBF information is required. Using a ground truth of O-15 PET rΔCBF in a cohort of Moyamoya disease patients (a condition with chronic narrowing of brain arteries leading to increased stroke risk), they showed that using the baseline MRI alone resulted in better performance at predicting regions with compromised CVR than the current clinical method using ASL before and after acetazolamide injection. Such a method may find use in estimating CVR from routine MRI scans acquired as part of clinical practice, obviating the need for either PET or acetazolamide.

3   Hemorrhagic Stroke or Intracranial Hemorrhage

Hemorrhagic stroke, also known as intracranial hemorrhage, accounts for approximately 13% of all strokes. Hemorrhagic stroke was found to have similar total death (three million yearly) and disability (69 million disability-adjusted life year) than ischemic stroke, although the incidence of ischemic stroke was twice as great [96]. Hemorrhagic stroke is commonly diagnosed through non-contrast CT or MRI (GRE or SWI are particularly sensitive to hemorrhage). Important considerations on the diagnosis and triaging include the presence, location, volume, and expansion of the hemorrhage. Chilamkurthy et al. [97] trained a ResNet with a large dataset of 300,000 CT scans to detect critical findings on CT including hemorrhage. The model was tested on 500 CT scans with high AUCs for detecting hemorrhage. However, the performance was not as good as expert radiologists. Lee et al. [98] proposed an ImageNet pre-trained deep CNN that was further trained on 904 CT cases of acute intracranial hemorrhage to detect hemorrhage and classify the 5 subtypes of hemorrhage. They tested in independent test datasets with about 400 cases and found the model achieved similar performance to expert radiologists with a sensitivity of 92–98% and specificity of 95%. In addition, the researchers attempted to explain this CNN model using the attention map, which showed that the model had a similar process that mimics the radiologists' workflow. Kuo et al. [99] trained a CNN with over 4000 head CT scans to classify and segment intracranial hemorrhages. They showed the model achieved an AUC of 0.991 on 200-case independent test set, with good performance in case with very small and subtle hemorrhagic lesions.

Machine learning has also been applied to diagnose the etiology of intracranial hemorrhage, examples including microbleeds, vascular malformation, and intracranial aneurysms. These topics are reviewed in separate sections.

4   Cerebral Vascular Malformation

Cerebral vascular malformations occur in 0.1–4.0% of the general population. Arteriovenous malformations (AVMs) are the most dangerous cerebral vascular malformation and can cause hemorrhage, seizures, headaches, and focal neurologic deficits.

Identifying intraparenchymal hemorrhage caused by AVMs on non-contrast-enhanced CT could be useful in triaging patients to appropriate treatment. Zhang et al. [100] selected radiomic features from 11 filter-based feature selection methods and applied multiple supervised machine learning algorithms to classify the intraparenchymal hemorrhage as AVM-related or other etiology. The best model was AdaBoost classifier, which achieved an AUC of 0.957, a sensitivity of 88.9%, and a specificity of 93.7% in the test set.

Stereotactic radiosurgery is most successful when used to treat small AVMs (diameter <3 cm) or in deep and eloquent areas that would engender great neurologic risk with attempted resection. Its performance relies on the accuracy of delineating the target AVM, since partial volume irradiation may result in obliteration failure and remained symptoms. Recently, Wang et al. [101] proposed a three-dimensional V-Net to automatically segment the AVMs on contrast CT images to guide stereotactic radiosurgery. They compared the V-Net model performance with human readers and achieved an average DSC of 0.85 and an average volume error of 0.076 mL among 80 patients.

Adverse radiation effects after stereotactic radiosurgery include cyst formation which may require surgical intervention and radiation-induced changes which may lead to permanent neurological deficits in 1–3% of the patients. Deep AVMs (located in the thalamus, basal ganglia, and brainstem), large AVMs, large radiation treatment volume, and repeated radiosurgery are risk factors to develop neurologic deficits after radiosurgery. Lee et al. [102] proposed an unsupervised classification with fuzzy c-means clustering to analyze the AVM nidus on T2-weighted MRI and analyzed the association between brain parenchyma component near the nidus and radiation-induced changes. The model automatically segmented nidus, brain parenchyma, and cerebrospinal fluid components in the radiation-exposed region. Compared with manual segmentation, the proposed algorithm achieved a DSC of 0.795. The automatically segmented brain parenchyma was associated with radiation-induced changes.

5   Intracranial Aneurysms

Intracranial aneurysms (IAs) have a prevalence of 3.2% in the general population [103, 104]. IA rupture accounts for 80–90% of spontaneous subarachnoid hemorrhages [5, 105], which is usually a catastrophic event, with a mortality rate of 23–51% [4, 5] and permanent disability in 30–40% [4, 6]. Survivors often suffer from long-term neuropsychological deficits and decreased quality of life. Although DSA is the gold standard to diagnose an aneurysm, unruptured IAs can be detected with non-invasive imaging techniques such as MR angiography (MRA) or CT angiography (CTA). Early diagnosis of IAs can benefit from clinical management which may prevent their rupture [106, 107]. However, there are two unmet clinical needs for IA: diagnosis and management.

5.1   Difficulty in Aneurysm Detection

Because of the small size of IAs and the complexity of intracranial vessels, aneurysm detection can be time-consuming and requires subspecialty training. It renders two challenges. First, there is a suboptimal inter-observer agreement (kappa = 0.67–0.73) in the detection of IA from CTA and MRA [108]. The interpretation may vary depending on the level of expertise. Therefore, the sensitivity of detecting IA in CTA and MRA can range from 60% for a resident to 80% for a neuroradiologist [109]. Second, there is a high false-negative rate in detecting small aneurysms with diameter less than 5 mm. It has been reported that the sensitivity of detecting IAs of less than 5 mm is 57–70% [108, 110] for CTA and 35–58% for MRA [109, 110]. In comparison, the sensitivity of detecting IAs larger than 5 mm is 94% and 86% for CTA and MRA. Given all the difficulties mentioned above, there is a clinical need to have high-performance computer-assisted diagnosis (CAD) tools to aid in detection, increase efficiency, and reduce disagreement among observers which may potentially improve the clinical care of patients.

5.1.1   AI Algorithm for Intracranial Aneurysm Detection

There have been several studies showing that CAD program can automatically detect IA in MRA or CTA. The conventional CAD systems, based on manually designed imaging features, such as vessel curvature, thresholding, or a region-growing algorithm, have shown good performance in detecting IA [111, 112]. However, these conventional methods were developed on very small datasets and had to be modified manually when applied to new images. New deep learning-based methods directly learn the most predictive features from a large dataset of labeled images. They have better performance and greater generalizability than conventional methods. Deep learning has also been used for IA detection in MRA and CTA, and several studies have shown decent results [113–116].

The diagnostic accuracy of models using various imaging modalities has been studied. Digital subtraction angiography (DSA), an invasive vascular imaging procedure, is the gold standard to diagnose an aneurysm. Zeng et al. [117] applied 2D CNN on 3D DSA by concatenating five consecutive rotational angles of the DSA image patch as model input. The model reached an accuracy of 99%. Duan et al. [118] performed a similar task but on 2D DSA. It is more difficult due to less identifiable features in the 2D projection image, especially the differentiation between the vessel overlaps and an aneurysm. They proposed a two-stage detection system: First, the neural network localized the target region on the DSA using feature pyramid network. Second, the anchor box of aneurysm and vessel overlaps was generated by dual input of anterior-posterior view and lateral view into another feature pyramid network. The model reached an AUC of 93.5%.

MRA and CTA offer non-invasive diagnosis of intracranial aneurysms. Nakao et al. [113] and Sichtermann et al. [119] showed the feasibility of using CNN for aneurysm detection on time-of-flight (TOF) MRA. More recently, Ueda et al. [114] trained a ResNet-18 model to detect aneurysms on using 683 TOF MRAs. The model was tested on both internal data and external data with sensitivity and specificity above 90%. Park et al. [115] proposed a 3D CNN with a encoder-decoder structure to segment the intracranial aneurysms from CT angiography. Similar to U-Net, the model contains skip connections to transmit output directly from the encoder to the decoder. The encoder was pre-trained using videos labeled with human actions. The model was trained, validated, and tested using 611, 92, and 115 CTAs. Augmenting physicians with artificial intelligence-produced segmentation resulted in improvement in sensitivity, accuracy, and interrater agreement when compared with no augmentation. Faron et al. [120] showed similar results in 3D TOF MRA with a smaller dataset.

5.2 Difficulties in Aneurysm Risk Evaluation

Once an IA is detected in imaging study, clinicians must determine how to manage an unruptured IA. Overall, IAs have a low annual rupture risk of 0.95% [121]. Current treatments to prevent IA rupture include open neurosurgical clipping or endovascular embolization; both have a relatively high peri-operative risk of stroke and death (3–10%) [122]. Therefore, the management of unruptured aneurysm remains controversial [123]. Currently, the decision on whether to intervene is mainly based on aneurysm size. If an IA is larger than 5 mm in diameter in the anterior cerebral circulation or larger than 7 mm in the posterior circulation, surgical treatment is considered [123]. If an IA is smaller than these thresholds, follow-up observation with serial imaging is typically pursued [124]. Change in size of an IA during the follow-up period is a warning sign of impending rupture and often leads to surgical or

endovascular treatment. However, IA rupture depends on multiple factors in addition to size, including aneurysm shape and location as well as hemodynamics of the aneurysm, blood pressure, and mental and physical stress of the patient [121, 125]. It is not optimal to make the decision to intervene solely on size criteria, given risk of rupture is multifactorial. Moreover, follow-up serial imaging takes time, and rupture may occur during the observation period [126–128].

5.2.1   AI-Based Aneurysm Risk Prediction Model

A more comprehensive morphological evaluation of IA would be optimal; it ideally would include data on aneurysm shape, geometry, presence of a daughter sac, volume, and comparison of IA morphology across serial scans. Deep learning-based methods have the potential to automatically perform precise IA segmentation and provide efficient tools for the morphological evaluation of IA. Furthermore, machine learning methods can take high-dimensional, cross-domain inputs and directly learn from the labeled data to construct sophisticated prediction models. Feature ranks derived from the machine learning model could provide (? information) on individual factors that can influence model prediction.

Several studies have attempted to segment aneurysms using deep learning [129, 130]. Podgorsak et al. [130] used a CNN with encoder and decoder architecture to segment aneurysms on DSA, achieving a DSC above 0.9 for intracranial aneurysms.

Optimization of treatment decisions for unruptured small aneurysms [and patients with multiple aneurysms] is needed. Studies have applied machine learning algorithms to predict the outcomes of unruptured aneurysms [131–137]. Liu et al. [132] used morphologic features derived from DSA and machine learning models to predict if an aneurysm was unstable (defined as rupture within 1 month), aneurysm growth, and symptomatic aneurysms. They found that aneurysms with a diameter between 4 and 8 mm and irregular morphology indicate the aneurysm instability with an area under curve (AUC) of 0.85 in a separate test set. Similarly, Kim et al. [133] used CNN on small aneurysms based upon rotational DSA and showed that the model had better performance on the prediction of aneurysm rupture than human predictions.

Tanioka et al. used machine learning-based methods with morphological and hemodynamic parameters as inputs to achieve relatively high accuracy (71.2–78.3%) in predicting rupture status of IA [138]. They found projection ratio, irregular shape, and size ratio were important for the discrimination of ruptured aneurysms. Shi et al. further included clinical data to morphologic and hemodynamic information, to construct a machine learning model to predict IA rupture and reported areas under the curve of 0.88–0.91 [139].

After aneurysm rupture, predicting common complications of aneurysmal subarachnoid hemorrhage such as vasospasm, delayed cerebral ischemia, and functional outcome could help guide patient care. Kim et al. [140] used clinical factors and morphological features of an aneurysm to predict vasospasm after IA rupture with a random forest regressor. The model achieved an accuracy rate of 0.855 (AUC of 0.88). Ramos et al. [141] used clinical and CT image features to predict delayed cerebral ischemia using multiple machine learning algorithms. The best model reached an AUC of 0.74. Similarly, Rubbert et al. [142] used clinical and imaging features to predict 6-month dichotomized modified Rankin scale using random forest, with an accuracy of 71%.

6 Cerebral Small Vessel Disease

Cerebral small vessel disease (cSVD) encompasses a spectrum of disorders affecting the brain's small perforating arterioles, capillaries, and probably venules [143], which cause various focal and global brain lesions that can be detected on pathological examination and brain imaging [144]. cSVD has a wide range of clinical manifestations. Although many affected patients may remain asymptomatic, cSVD may herald patients at risk for acute ischemic stroke or intracerebral hemorrhage; it can also present as an insidious clinical course associated with progressive cognitive decline, development of mood disorders, and gait disturbance [145]. cSVD causes about one-fourth of all acute ischemic strokes and is a major risk factor for hemorrhagic strokes [146–148]. It is the most common cause of vascular dementia and mixed dementia, which often occurs with Alzheimer's disease, and contributes to about one-half of all dementias worldwide, thus causing a massive health burden [146, 149, 150].

6.1 Imaging Features of cSVD

Neuroimaging plays a pivotal role in the diagnosis and evaluation of cSVD [143]. According to the STandards for ReportIng Vascular changes on nEuroimaging (STRIVE), the imaging features of cSVD include recent small subcortical infarcts, white matter hyperintensities (WMH) of presumed vascular origin, lacunes, enlarged perivascular spaces (PVS), and cerebral microbleeds (CMBs) (Fig. 4) [144]. These imaging findings, either individually or in combination, are associated with cognitive impairment, dementia, depression, mobility problems, increased risk of stroke, and worse outcomes after stroke [146, 151–153]. The quantification of cSVD imaging features is important for disease severity evaluation and clinical prognostication [154, 155]. However, these lesions are generally small and widespread in the brain, rendering manual inspection and segmentation laborious and prone to error. Machine learning algorithms have great potential in the automatic
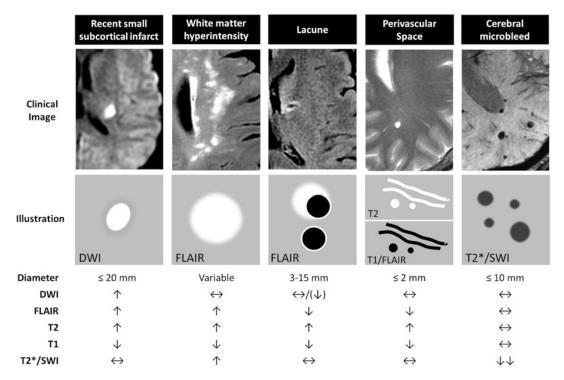
Fig. 4 MR imaging features for cerebral small vessel disease. (Upper) Clinical images (upper) and illustrations (middle) of MRI features for cerebral small vessel disease, with a summary of imaging characteristics (lower) for individual features. DWI, diffusion-weighted imaging. FLAIR, fluid-attenuated inversion recovery. SWI, susceptibility-weighted imaging. ↑, increased signal. ↓, decreased signal. ↔, iso-intense signal. (The figure is reproduced based on reference Wardlaw et al. [145])

quantification of the cSVD imaging features. A "total cSVD score" of the brain could be calculated by combining all pertinent features and may better represent the disease status and burden of cSVD. Such applications could help with disease diagnosis, treatment, monitoring, and prognostication in patients with cSVD.

We will review current machine learning applications for the detection and quantification of cSVD imaging features, including WMH, CMB, lacune, and PVS, as well as the total burden of cSVD.

6.2 White Matter Hyperintensity Segmentation

WMH of presumed vascular origin, characterized by hyperintense lesions on fluid-attenuated inversion recovery (FLAIR) MRI within the white matter, is one of the main features of cSVD [144]. These abnormalities play a key role in normal aging, dementia, and stroke. Large longitudinal population-based studies have confirmed a dose-dependent relationship between WMH volume and clinical outcome, making its measurement of clinical interest [156]. The Fazekas visual rating scale is the most widely used method to assess WMH burden in the clinical setting; it is a four-grade scale rating the size and confluence of WMH lesions in periventricular and deep white matter (Fig. 5) [157]. However, the Fazekas scale has high
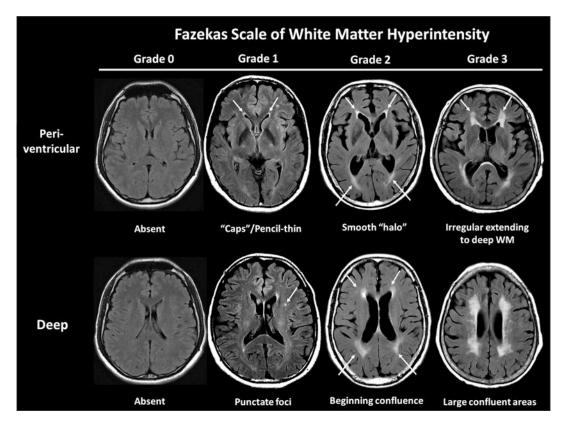
Fig. 5 The Fazekas visual rating scale for white matter hyperintensity. A four-grade scale depending on the size and confluence of lesions is given in the periventricular (upper) and deep white matter (lower) regions, respectively

intra- and inter-subject variability [158], significant ceiling/floor effects [159], and poor sensitivity to clinical group differences [160], leading to inconsistencies in WMH research.

Segmentation and quantification of WMH lesion volume are needed. Before the emergence of deep learning techniques, many automatic WMH segmentation methods were proposed, including supervised methods, e.g., k-nearest neighbors [161], support vector machine [162], Bayesian method based on signal intensity and spatial information [162] or multi-contrast image [163], combined morphological segmentation and adaptive boosting classifier [164], and artificial neural network [165], and unsupervised method, e.g., histogram analysis [166], fuzzy classification algorithm [167, 168], Gaussian mixture model [169], and hidden Markov random field model [170]. However, these methods were generally limited to specific imaging modalities and patient characteristics (e.g., age, clinical presentation) and used different metrics for analysis, making it hard to compare methods to one another [171].
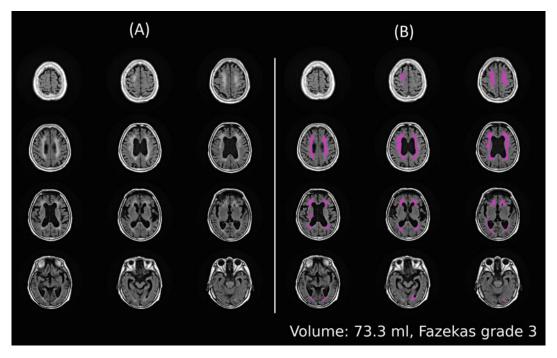
Fig. 6 Example of white matter hyperintensity (WMH) segmentation and quantification. (**a**) The original T2 FLAIR image. (**b**) Automatic WMH segmentation (pink areas) and volume quantification can be achieved by deep learning algorithm which provides a more precise estimation of WMH burden in the brain than the Fazekas scale. WMH white matter hyperintensity

6.2.1 Deep Learning-Based Methods for WMH Segmentation

The WMH Segmentation Challenge at the Medical Image Computing and Computer Assisted Intervention Society (MICCAI) 2017 (https://wmh.isi.uu.nl/) provided a standardized assessment of automatic methods for WMH segmentation. The multi-center/multi-scanner dataset comprised images from patients with various degrees of age-related degenerative and vascular pathologies. The training dataset included 60 images from 3 scanners, with manual WMH segmentation by 2 experts as the ground truth. The testing dataset included 110 images obtained from 5 MR scanners, including data from 2 scanners not used in the training set, to evaluate the generalizability of segmentation methods on untested (?) scanners. Five evaluation metrics, including DSC, modified Hausdorff distance, volume difference, sensitivity, and F1 for detecting individual lesion, were used to rank the methods. Among the 20 participants, all the top 10 participants applied deep learning methods [172]. The top-ranking methods performed similarly or better than the two independent human observers, who did not serve as the raters of the ground truth, suggesting the potential of automatic methods to replace human raters (Fig. 6). Li et al. [173], the winner, achieved a DSC of 0.8 and a recall of 0.84 by utilizing an ensemble of three fully convolutional neural networks similar to U-Net with different initializations. Of note, they removed the

WMH prediction in the first and last 1/8 slices, where false-positive prediction frequently occurred, as a post-processing method. Andermatt et al. [174], in second place, utilized a network based on multi-dimensional gated recurrent units (GRU), trained on 3D patches, to achieve a DSC of 0.78 and a recall of 0.83. Ghafoorian et al. [175], in third place, constructed a multi-scale 2D CNN, trained in tenfolds and selecting the three best performing checkpoints on the training data, to achieve a DSC of 0.77, a recall of 0.73, and the highest F1 score of 0.78. Valverde et al. [176], in fourth, constructed a cascade framework of three 3D CNNs, with the first model to identify candidate lesion voxels, the second to reduce false-positive detections, and the third to perform final WMH segmentation. Overall, challenge results indicate that ensemble methods and strategies for false-positive reduction, including selective sampling WMH mimics, removing slices prone to false positives, and adding false-positive reduction model, are advantageous. The top-ranking models generally had very few false positives in normal areas that are hyperintense on FLAIR but are not WMH (e.g., the septum pellucidum), a fault of many lower-ranking methods. Although the top-four ranking models remained to be the leaders in the inter-scanner robustness ranking, some higher-ranking, deep learning-based methods performed worse in inter-scanner robustness than the lower-ranking, rule-based methods, suggesting data-driven approaches sometimes may not generalize well to unseen scanners.

The WMH Segmentation Challenge remains open for new and updated submissions. Zhang et al. [177] designed a dual-path U-Net segmentation model that used an attention mechanism to combine FLAIR sequences and a brain atlas (for location information) inputs to achieve higher performance than the previously mentioned methods. Park et al. [178] proposed a U-Net with multi-scale highlighting foregrounds, which was designed to improve the detection of the WMH voxels with partial volume effects, and achieved a record high of DSC (0.81) and F1 score (0.79).

Although deep learning methods are gaining popularity and have shown great performance in the WMH Segmentation Challenge, a recent systemic review [179] of automatic WMH segmentation methods developed from 2015 to July 2020 showed no evidence to favor deep learning methods in clinical research over the k-NN algorithm [180, 181], linear regression [182, 183], or unsupervised methods (e.g., fuzzy c-means algorithm [184, 185], Gaussian mixture model [186], statistical definition [187]), in terms of spatial agreement with reference segmentations (i.e., DSC). Non-deep learning methods, such as k-NN and linear regression methods, have the advantage of simplicity, can be easier to train, and may be less susceptible to overfitting when dealing

with a limited amount of training data. Future research requires high-quality large-sized open data and code availability to overcome bias in study design and ground truth generation in order to fully compare and validate these methods [188].

6.3 Cerebral Microbleed (CMB) Detection

CMBs are radiological manifestations of cerebral small vessel disease, usually defined as small (≤10 mm) areas of signal void on T2∗-weighted gradient-recalled echo (GRE) or susceptibility-weighted images (SWI). CMBs are frequently seen in patients with spontaneous intracranial hemorrhage [189] or cognitive impairment [189] and are associated with a higher risk of hemorrhage after IV thrombolysis or therapeutic anticoagulation [190, 191]. CMBs are highly associated with underlying uncontrolled hypertension (particularly when located in deep and/or posterior fossa structures) [192] and/or cerebral amyloid angiopathy (especially when seen in cortical locations) [193]. Detecting CMBs can be clinically important to assess the benefits and risks in treatment planning for stroke patients.

Greenberg et al. [189] published a detailed field guide to CMB detection. The small size of CMBs and the existence of several CMB mimics (e.g., small veins, calcifications, cavernous malformations, iron deposition in deep nucleus, and flow voids) lead to limited inter-observer agreement, long scan interpretation time, and increased error rate by manual inspection, especially for patients with heavy CMB load.

Automatic CMB detection methods might improve the efficiency and accuracy of CMB identification. Radiomic-based and traditional machine learning automatic detection methods have been investigated. Van den Heuvel et al. [194] used morphological features based on the dark and spherical nature of CMBs and random forest classifier to achieve a sensitivity of 89.1% and 25.9 false positives per subject on CMB detection. Several studies have applied deep learning models to improve CMB detection [195–198]. Dou et al. [198] utilized a two-step cascade framework, first with a 3D fully convolutional network for the screening of CMB candidates, followed by a 3D CNN discriminator for the exclusion of CMB mimics, to achieve a sensitivity of 93.16%, precision of 44.31%, and 2.74 false positives per subject for the detection of CMB on SWI. Liu et al. [196] used a two-stage 3D CNN architecture, while adding phase images to SWI as model inputs. The phase images enabled the differentiation of diamagnetic calcifications from paramagnetic CMB, which is not a distinction radiologists can make solely on SWI. Their model successfully reduced false-positive detection and achieved a sensitivity of 95.8%, precision of 70.9%, and 1.6 false positives per subject. Rashid et al. further added quantitative susceptibility mapping (QSM) to SWI as inputs to construct a multi-class U-Net CNN method to differentiate CMBs and non-hemorrhage iron deposits, which was not

achievable with SWI and phase images [197]. The multi-class model reached a sensitivity of 84% and a precision of 59% for CMB detection and a sensitivity of 75% and a precision of 75% for iron deposit detection.

6.4 Lacune Lesion Detection

Lacunes of presumed vascular origin are sequelae of chronic small subcortical infarcts or hemorrhages located in deep gray and white matter in the territory of a perforating arteriole [144]. They are associated with an increased risk of stroke, dementia, and gait impairment [143, 144]. In neuroimaging, lacunes appear as round or ovoid, subcortical, fluid-filled cavities, measuring between 3 and 15 mm, typically showing a surrounding hyperintense gliotic rim on T2 FLAIR images [144]. Longitudinal spatial mapping studies show new WMH forming around small subcortical infarcts [199] and new lacunes forming at the margin of WMH [200], suggesting a strong association and vicinity between the two types of lesions. Therefore, automatic applications that can not only segment WMH but also detect lacunes are desired. However, few studies have proposed automatic methods for lacune detection. Uchiyama et al. [201] developed an algorithm that first used top-hat transformation and multiple-phase binarization techniques to detect potential candidates of lacune and then used rule-based schemes and a support vector machine to eliminate the false positives to achieve a sensitivity of 96.8% with 0.76 false positive per slice. Wang et al. [169] applied a multi-step algorithm to detect WMH, cortical infarcts, and lacunes. The steps included extraction of brain tissue, segmentation of hyperintense lesions from brain tissue using Gaussian mixture model, separation of WMH and cortical infarct based on anatomical location and morphological operation, and segmentation of lacunes based on location and intensity threshold. They achieved a sensitivity of 83.3% with 0.06 false positives per subject for lacune detection. Ghafoorian et al. [202] used a two-stage deep learning method, which included a fully convolutional neural network for candidate detection and a 3D multi-scale location-aware CNN for false-positive reduction. The method achieved a sensitivity of 97.4% with 0.13 false positives per slice.

6.5 Perivascular Space Quantification

Perivascular spaces (PVS), also known as Virchow-Robin spaces, are extensions of extracerebral fluid spaces that surround the penetrating vessels of the brain [144]. They were recently recognized as parts of the glymphatic system, which is a brain-wide perivascular fluid transport system responsible for the clearance of waste in the brain [203]. Normal PVS are not typically seen on conventional MRI, while enlarged PVS are associated with progression of subcortical infarcts, WMH, CMBs, and cognitive decline and are considered a biomarker for cSVD [204]. In neuroimaging, PVS appear as round or ovoid cavities with diameters less than

3 mm and demonstrate signal intensity identical to that of CSF. They are typically located in the inferior basal ganglia, centrum semiovale, and midbrain. PVS may look similar to lacunes on MRI. However, PVS do not have a surrounding gliotic rim and appear more elongated when imaged parallel to the course of the penetrating vessel. The severity of PVS can be graded by a widely used visual rating scale according to Charidimou et al., which is a four-point grade based on the total number of PVS (0, no PVS; 1 [mild], 1–10 PVS; 2 [moderate], 11–20 PVS; 3 [moderate to severe], 21–40 PVS; 4 [severe], > 40 PVS) in the basal ganglia and centrum semiovale [205]. Given the small size and the large number of PVS, it is extremely laborious and time-consuming to perform manual counting or segmentation of PVS, which may explain the scarcity of studies about automatic methods for PVS quantification in the literature. Park et al. [206] proposed a supervised method to perform automatic PVS segmentation method based on manually derived PVS masks on 7 T MR images. They extracted Haar-like features, which are often used in object recognition, from regions of interest determined by brain and vascular structure and used a random forest classifier to achieve a DSC of 0.73, sensitivity of 69%, and positive predictive value of 80%. Ballerini et al. [207] propose a PVS segmentation technique based on the 3D Frangi filtering. Because of the lack of ground truth of PVS segmentation mask, they alternatively optimized and evaluated the method by using ordered logit models and visual rating scales. The method achieved a Spearman's correlation coefficient of 0.74 ($p < 0.001$) between segmentation-based PVS burden and visual rating scale. Dubost et al. [208] used 3D convolutional neural network regression to predict visual rating scale and achieved an intraclass correlation coefficient of 0.75–0.88 between visual and automated scales, which was even higher than the inter-observer agreement among human raters.

6.6   Total Small Vessel Disease Burden

cSVD is considered a dynamic, whole brain disorder with a wide spectrum of clinical presentations and diffuse imaging manifestations in the brain while sharing common microvascular pathologies [209]. A multifactorial approach that combines all imaging features may better represent the burden and disease status of cSVD. Several visual scoring systems of total cSVD burden have been introduced [154, 205]. Staals et al. [154] proposed a four-point score in which one point is given in the presence of each of the cSVD imaging feature: (1) more than one lacune, (2) more than one microbleed, (3) moderate to severe (more than 11) PVS in basal ganglia, and (4) periventricular WMH Fazekas score of 3 and/or deep WMH Fazekas score of 2–3. Although these semiquantitative scoring systems are pragmatic and simple for clinical use, they have several limitations. First, they may not be sensitive enough to represent the severity of the disease, as the accumulation of cSVD burden forms a
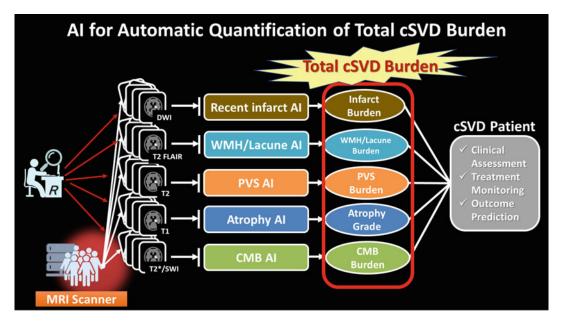
Fig. 7 AI applications for cerebral small vessel disease (cSVD). AI algorithms have great potential to perform automatic quantification of individual cSVD imaging features. By combining these burdens, a "total cSVD burden" could be quantified, which might facilitate the clinical assessment, treatment monitoring, and outcome prediction in patients with cSVD

continuum, rather than several ordinal scores. Second, visual scoring may be subjective and laborious for raters, especially for WMH and PVS evaluation. Third, existing scoring doesn't account for lesion location, but anatomical location is a known key factor for cognitive impairment [210]. The automatic methods for different cSVD imaging features described in the previous sections can offer quantitative measurements of the cSVD burden in the whole brain and are well suited to overcome these limitations. Several studies have shown great potential for computer-generated total cSVD burden in the assessment of cSVD patients. Duan et al. [211] developed a multiple CNN-based system that can accurately segment subcortical infarcts, CMBs, WMHs, and lacunes 4.4 s per subject. Dickie et al. [212] used a voxel-based Gaussian mixture model cluster analysis on multi-contrast MR images to estimate overall WMH, lacunes, CMBs, and atrophy into a "brain health index"; they showed the brain health index has a stronger association with cognitive outcome than WMH volume and visual cSVD score. Jokinen et al. [213] used automated atlas- and CNN-based segmentation methods to yield volumetric measures of WMHs, lacunes, PVS, cortical infarcts, and brain atrophy to show that the combined measure of all markers was a more powerful predictor of cognitive and functional outcomes than any individual measure alone.

Overall, previous studies have shown great potential of machine learning algorithms to perform automatic segmentation or detection of cSVD imaging features. By combining the measurement of each cSVD feature, a "total cSVD burden" can be quantified, which might be used to facilitate clinical assessment, treatment monitoring, and outcome prediction in patients with cSVD (Fig. 7).

7 Conclusion

In conclusion, machine learning algorithms show great potential in improving clinical diagnosis and care for cerebrovascular disorders. ML performance varies by study and dataset, but in many cases already exceeds the current clinical state-of-the-art [?measures]. There is a need for more large cohort validation studies, and the development of standard test sets for comparing different algorithms would enable fairer comparison between methods. In addition, more real-world experience is necessary to understand the role of machine learning in improving the diagnosis and care of cerebrovascular disorders.

Acknowledgments

References

1. Virani SS, Alonso A, Aparicio HJ, Benjamin EJ, Bittencourt MS, Callaway CW et al (2021) Heart disease and stroke Statistics-2021 update: a report from the American Heart Association. Circulation 143(8):e254–e743. https://doi.org/10.1161/CIR.0000000000000950

2. Collaborators GBDS (2021) Global, regional, and national burden of stroke and its risk factors, 1990-2019: a systematic analysis for the global burden of disease study 2019. Lancet Neurol 20(10):795–820. https://doi.org/10.1016/S1474-4422(21)00252-0

3. Cannistraro RJ, Badi M, Eidelman BH, Dickson DW, Middlebrooks EH, Meschia JF (2019) CNS small vessel disease: a clinical review. Neurology 92(24):1146–1156. https://doi.org/10.1212/WNL.0000000000007654

4. Ingall T, Asplund K, Mähönen M, Bonita R (2000) A multinational comparison of subarachnoid hemorrhage epidemiology in the WHO MONICA stroke study. Stroke 31(5):1054–1061. https://doi.org/10.1161/01.str.31.5.1054

5. van Gijn J, Kerr RS, Rinkel GJE (2007) Subarachnoid haemorrhage. Lancet (London, England) 369(9558):306–318. https://doi.org/10.1016/S0140-6736(07)60153-6

6. Hop JW, Rinkel GJ, Algra A, van Gijn J (1997) Case-fatality rates and functional outcome after subarachnoid hemorrhage: a systematic review. Stroke 28(3):660–664. https://doi.org/10.1161/01.str.28.3.660

7. Saver JL, Goyal M, van der Lugt A, Menon BK, Majoie CB, Dippel DW et al (2016) Time to treatment with endovascular thrombectomy and outcomes from ischemic stroke: a meta-analysis. JAMA 316(12):1279–1288. https://doi.org/10.1001/jama.2016.13647

8. Powers WJ, Rabinstein AA, Ackerson T, Adeoye OM, Bambakidis NC, Becker K et al (2019) Guidelines for the early management of patients with acute ischemic stroke: 2019

update to the 2018 guidelines for the early management of acute ischemic stroke: a guideline for healthcare professionals from the American Heart Association/American Stroke Association. Stroke 50(12):e344–e418. https://doi.org/10.1161/STR.0000000000000211

9. Rennert RC, Wali AR, Steinberg JA, Santiago-Dieppa DR, Olson SE, Pannell JS et al (2019) Epidemiology, natural history, and clinical presentation of large vessel ischemic stroke. Neurosurgery 85(suppl_1):S4–S8. https://doi.org/10.1093/neuros/nyz042

10. Goyal M, Menon BK, van Zwam WH, Dippel DW, Mitchell PJ, Demchuk AM et al (2016) Endovascular thrombectomy after large-vessel ischaemic stroke: a meta-analysis of individual patient data from five randomised trials. Lancet 387(10029):1723–1731. https://doi.org/10.1016/S0140-6736(16)00163-X

11. Badhiwala JH, Nassiri F, Alhazzani W, Selim MH, Farrokhyar F, Spears J et al (2015) Endovascular thrombectomy for acute ischemic stroke: a meta-analysis. JAMA 314(17):1832–1843. https://doi.org/10.1001/jama.2015.13767

12. Hassan AE, Ringheanu VM, Rabah RR, Preston L, Tekle WG, Qureshi AI (2020) Early experience utilizing artificial intelligence shows significant reduction in transfer times and length of stay in a hub and spoke model. Interv Neuroradiol 26(5):615–622. https://doi.org/10.1177/1591019920953055

13. Yahav-Dovrat A, Saban M, Merhav G, Lankri I, Abergel E, Eran A et al (2021) Evaluation of artificial intelligence-powered identification of large-vessel occlusions in a comprehensive stroke center. AJNR Am J Neuroradiol 42(2):247–254. https://doi.org/10.3174/ajnr.A6923

14. Stib MT, Vasquez J, Dong MP, Kim YH, Subzwari SS, Triedman HJ et al (2020) Detecting large vessel occlusion at multiphase CT angiography by using a deep convolutional neural network. Radiology 297(3):640–649. https://doi.org/10.1148/radiol.2020200334

15. Dehkharghani S, Lansberg M, Venkatsubramanian C, Cereda C, Lima F, Coelho H et al (2021) High-performance automated anterior circulation CT angiographic clot detection in acute stroke: a multi-reader comparison. Radiology 298(3):665–670. https://doi.org/10.1148/radiol.2021202734

16. You J, Yu PLH, Tsang ACO, Tsui ELH, Woo PPS, Leung GKK (2019) Automated computer evaluation of acute ischemic stroke and large vessel occlusion. arXiv preprint arXiv:1906.08059

17. You J, Tsang ACO, Yu PLH, Tsui ELH, Woo PPS, Lui CSM et al (2020) Automated hierarchy evaluation system of large vessel occlusion in acute ischemia stroke. Front Neuroinform 14:13. https://doi.org/10.3389/fninf.2020.00013

18. Olive-Gadea M, Crespo C, Granes C, Hernandez-Perez M, Perez de la Ossa N, Laredo C et al (2020) Deep learning based software to identify large vessel occlusion on noncontrast computed tomography. Stroke 51(10):3133–3137. https://doi.org/10.1161/STROKEAHA.120.030326

19. Gaha M, Roy C, Estrade L, Gevry G, Weill A, Roy D et al (2014) Inter- and intraobserver agreement in scoring angiographic results of intra-arterial stroke therapy. AJNR Am J Neuroradiol 35(6):1163–1169. https://doi.org/10.3174/ajnr.A3828

20. Volny O, Cimflova P, Szeder V (2017) Inter-Rater reliability for thrombolysis in cerebral infarction with TICI 2c category. J Stroke Cerebrovasc Dis 26(5):992–994. https://doi.org/10.1016/j.jstrokecerebrovasdis.2016.11.008

21. Ueda D, Katayama Y, Yamamoto A, Ichinose T, Arima H, Watanabe Y et al (2021) Deep learning-based angiogram generation model for cerebral angiography without misregistration artifacts. Radiology 299(3):675–681. https://doi.org/10.1148/radiol.2021203692

22. Zhang M, Zhang C, Wu X, Cao X, Young GS, Chen H et al (2020) A neural network approach to segment brain blood vessels in digital subtraction angiography. Comput Methods Prog Biomed 185:105159. https://doi.org/10.1016/j.cmpb.2019.105159

23. Bhurwani MMS, Snyder KV, Waqas M, Mokin M, Rava RA, Podgorsak AR et al (2021) Use of biplane quantitative angiographic imaging with ensemble neural networks to assess reperfusion status during mechanical thrombectomy. Proc SPIE Int Soc Opt Eng 11597:115971F

24. Su R, Cornelissen SAP, van der Sluijs M, van Es A, van Zwam WH, Dippel DWJ et al (2021) autoTICI: automatic brain tissue reperfusion scoring on 2D DSA images of acute ischemic stroke patients. IEEE Trans Med Imaging 40(9):2380–2391. https://doi.org/10.1109/TMI.2021.3077113

25. Su R, van der Sluijs M, Cornelissen SAP, Lycklama G, Hofmeijer J, Majoie C et al (2022) Spatio-temporal deep learning for automatic detection of intracranial vessel perforation in digital subtraction angiography during endovascular thrombectomy. Med Image Anal 77:102377. https://doi.org/10.1016/j.media.2022.102377

26. Wang J, Zhang J, Gong X, Zhang W, Zhou Y, Lou M (2022) Prediction of large vessel occlusion for ischaemic stroke by using the machine learning model random forests. Stroke Vasc Neurol 7(2):94–100. https://doi.org/10.1136/svn-2021-001096

27. Chen Z, Zhang R, Xu F, Gong X, Shi F, Zhang M et al (2018) Novel prehospital prediction model of large vessel occlusion using artificial neural network. Front Aging Neurosci 10:181. https://doi.org/10.3389/fnagi.2018.00181

28. Tarkanyi G, Tenyi A, Hollos R, Kalmar PJ, Szapary L (2022) Optimization of large vessel occlusion detection in acute ischemic stroke using machine learning methods. Life (Basel) 12(2):230. https://doi.org/10.3390/life12020230

29. Uchida K, Kouno J, Yoshimura S, Kinjo N, Sakakibara F, Araki H et al (2022) Development of machine learning models to predict probabilities and types of stroke at prehospital stage: the Japan urgent stroke triage score using machine learning (JUST-ML). Transl Stroke Res 13(3):370–381. https://doi.org/10.1007/s12975-021-00937-x

30. Hayashi Y, Shimada T, Hattori N, Shimazui T, Yoshida Y, Miura RE et al (2021) A prehospital diagnostic algorithm for strokes using machine learning: a prospective observational study. Sci Rep 11(1):20519. https://doi.org/10.1038/s41598-021-99828-2

31. Thomalla G, Simonsen CZ, Boutitie F, Andersen G, Berthezene Y, Cheng B et al (2018) MRI-guided thrombolysis for stroke with unknown time of onset. N Engl J Med 379(7):611–622. https://doi.org/10.1056/NEJMoa1804355

32. Mackey J, Kleindorfer D, Sucharew H, Moomaw CJ, Kissela BM, Alwell K et al (2011) Population-based study of wake-up strokes. Neurology 76(19):1662–1667. https://doi.org/10.1212/WNL.0b013e318219fb30

33. Fink JN, Kumar S, Horkan C, Linfante I, Selim MH, Caplan LR et al (2002) The stroke patient who woke up: clinical and radiological features, including diffusion and perfusion MRI. Stroke 33(4):988–993. https://doi.org/10.1161/01.str.0000014585.17714.67

34. Xu XQ, Zu QQ, Lu SS, Cheng QG, Yu J, Sheng Y et al (2014) Use of FLAIR imaging to identify onset time of cerebral ischemia in a canine model. AJNR Am J Neuroradiol 35(2):311–316. https://doi.org/10.3174/ajnr.A3689

35. Thomalla G, Rossbach P, Rosenkranz M, Siemonsen S, Krutzelmann A, Fiehler J et al (2009) Negative fluid-attenuated inversion recovery imaging identifies acute ischemic stroke at 3 hours or less. Ann Neurol 65(6):724–732. https://doi.org/10.1002/ana.21651

36. Petkova M, Rodrigo S, Lamy C, Oppenheim G, Touze E, Mas JL et al (2010) MR imaging helps predict time from symptom onset in patients with acute stroke: implications for patients with unknown onset time. Radiology 257(3):782–792. https://doi.org/10.1148/radiol.10100461

37. Lee H, Lee EJ, Ham S, Lee HB, Lee JS, Kwon SU et al (2020) Machine learning approach to identify stroke within 4.5 hours. Stroke 51(3):860–866. https://doi.org/10.1161/STROKEAHA.119.027611

38. Zhu H, Jiang L, Zhang H, Luo L, Chen Y, Chen Y (2021) An automatic machine learning approach for ischemic stroke onset time identification based on DWI and FLAIR imaging. Neuroimage Clin 31:102744. https://doi.org/10.1016/j.nicl.2021.102744

39. Ho KC, Speier W, Zhang H, Scalzo F, El-Saden S, Arnold CW (2019) A machine learning approach for classifying ischemic stroke onset time from imaging. IEEE Trans Med Imaging 38(7):1666–1676. https://doi.org/10.1109/TMI.2019.2901445

40. Ho KC, Speier W, El-Saden S, Arnold CW (2017) Classifying acute ischemic stroke onset time using deep imaging features. AMIA Annu Symp Proc 2017:892–901

41. Pexman JH, Barber PA, Hill MD, Sevick RJ, Demchuk AM, Hudon ME et al (2001) Use of the Alberta stroke program early CT score (ASPECTS) for assessing CT scans in patients with acute stroke. AJNR Am J Neuroradiol 22(8):1534–1542

42. Yoshimura S, Sakai N, Yamagami H, Uchida K, Beppu M, Toyoda K et al (2022) Endovascular therapy for acute stroke with a large ischemic region. N Engl J Med. https://doi.org/10.1056/NEJMoa2118191

43. Chen L, Bentley P, Rueckert D (2017) Fully automatic acute ischemic lesion segmentation in DWI using convolutional neural networks. Neuroimage Clin 15:633–643. https://doi.org/10.1016/j.nicl.2017.06.016

44. Wu O, Winzeck S, Giese AK, Hancock BL, Etherton MR, Bouts M et al (2019) Big data approaches to phenotyping acute ischemic stroke using automated lesion segmentation of multi-Center magnetic resonance imaging data. Stroke 50(7):1734–1741. https://doi.org/10.1161/STROKEAHA.119.025373

45. Maier O, Menze BH, von der Gablentz J, Hani L, Heinrich MP, Liebrand M et al (2017) ISLES 2015 - a public evaluation benchmark for ischemic stroke lesion segmentation from multispectral MRI. Med Image Anal 35:250–269. https://doi.org/10.1016/j.media.2016.07.009

46. Praveen GB, Agrawal A, Sundaram P, Sardesai S (2018) Ischemic stroke lesion segmentation using stacked sparse autoencoder. Comput Biol Med 99:38–52. https://doi.org/10.1016/j.compbiomed.2018.05.027

47. Tomita N, Jiang S, Maeder ME, Hassanpour S (2020) Automatic post-stroke lesion segmentation on MR images using 3D residual convolutional neural network, vol 27, p 102276

48. Liu L, Kurgan L, Wu FX, Wang J (2020) Attention convolutional neural network for accurate segmentation and quantification of lesions in ischemic stroke disease. Med Image Anal 65:101791. https://doi.org/10.1016/j.media.2020.101791

49. Karthik R, Gupta U, Jha A, Rajalakshmi R, Menaka R (2019) A deep supervised approach for ischemic lesion segmentation from multimodal MRI using fully convolutional network. Appl Soft Comput 84:105685. https://doi.org/10.1016/j.asoc.2019.105685

50. Liu L, Chen S, Zhang F, Wu F, Pan Y, Wang J (2020) Deep convolutional neural network for automatically segmenting acute ischemic stroke lesion in multi-modality MRI. Neural Comput Appl 32:6545

51. Zhang L, Song R, Wang Y, Zhu C, Liu J, Yang J et al (2020) Ischemic stroke lesion segmentation using multi-plane information fusion. IEEE Access 8:45715–45725. https://doi.org/10.1109/ACCESS.2020.2977415

52. Zhao B, Ding S, Wu H, Liu G, Cao C, Jin S, et al. (2019) Automatic acute ischemic stroke lesion segmentation using semi-supervised learning. https://doi.org/10.48550/arXiv.1908.03735

53. Federau C, Christensen S, Scherrer N, Ospel JM, Schulze-Zachau V, Schmidt N et al (2020) Improved segmentation and detection sensitivity of diffusion-weighted stroke lesions with synthetically enhanced deep learning. Radiol Artif Intell 2(5):e190217. https://doi.org/10.1148/ryai.2020190217

54. Woo I, Lee A, Jung SC, Lee H, Kim N, Cho SJ et al (2019) Fully automatic segmentation of acute ischemic lesions on diffusion-weighted imaging using convolutional neural networks: comparison with conventional algorithms. Korean J Radiol 20(8):1275–1284. https://doi.org/10.3348/kjr.2018.0615

55. Winzeck S, Mocking SJT, Bezerra R, Bouts M, McIntosh EC, Diwan I et al (2019) Ensemble of convolutional neural networks improves automated segmentation of acute ischemic lesions using multiparametric diffusion-weighted MRI. AJNR Am J Neuroradiol 40(6):938–945. https://doi.org/10.3174/ajnr.A6077

56. Do LN, Baek BH, Kim SK, Yang HJ, Park I, Yoon W (2020) Automatic assessment of ASPECTS using diffusion-weighted imaging in acute ischemic stroke using recurrent residual convolutional neural network. Diagnostics (Basel) 10(10):803. https://doi.org/10.3390/diagnostics10100803

57. Qiu W, Kuang H, Teleg E, Ospel JM, Sohn SI, Almekhlafi M et al (2020) Machine learning for detecting early infarction in acute stroke with non-contrast-enhanced CT. Radiology 294(3):638–644. https://doi.org/10.1148/radiol.2020191193

58. Kuang H, Najm M, Chakraborty D, Maraj N, Sohn SI, Goyal M et al (2019) Automated ASPECTS on noncontrast CT scans in patients with acute ischemic stroke using machine learning. AJNR Am J Neuroradiol 40(1):33–38. https://doi.org/10.3174/ajnr.A5889

59. Albers GW, Wald MJ, Mlynash M, Endres J, Bammer R, Straka M et al (2019) Automated calculation of Alberta stroke program early CT score: validation in patients with large hemispheric infarct. Stroke 50(11):3277–3279. https://doi.org/10.1161/STROKEAHA.119.026430

60. Maegerlein C, Fischer J, Monch S, Berndt M, Wunderlich S, Seifert CL et al (2019) Automated calculation of the Alberta stroke program early CT score: feasibility and reliability. Radiology 291(1):141–148. https://doi.org/10.1148/radiol.2019181228

61. Brinjikji W, Abbasi M, Arnold C, Benson JC, Braksick SA, Campeau N et al (2021) e-ASPECTS software improves interobserver agreement and accuracy of interpretation of aspects score. Interv Neuroradiol 27(6):781–787. https://doi.org/10.1177/15910199211011861

62. Neuhaus A, Seyedsaadat SM, Mihal D, Benson J, Mark I, Kallmes DF et al (2020)

Region-specific agreement in ASPECTS estimation between neuroradiologists and e-ASPECTS software. J Neurointerv Surg. 12(7):720–723. https://doi.org/10.1136/neurintsurg-2019-015442

63. Nagel S, Sinha D, Day D, Reith W, Chapot R, Papanagiotou P et al (2017) e-ASPECTS software is non-inferior to neuroradiologists in applying the ASPECT score to computed tomography scans of acute ischemic stroke patients. Int J Stroke 12(6):615–622. https://doi.org/10.1177/1747493016681020

64. Herweh C, Ringleb PA, Rauch G, Gerry S, Behrens L, Mohlenbruch M et al (2016) Performance of e-ASPECTS software in comparison to that of stroke physicians on assessing CT scans of acute ischemic stroke patients. Int J Stroke 11(4):438–445. https://doi.org/10.1177/1747493016632244

65. Hakim A, Christensen S, Winzeck S, Lansberg MG, Parsons MW, Lucas C et al (2021) Predicting infarct core from computed tomography perfusion in acute ischemia with machine learning: lessons from the ISLES challenge. Stroke 52(7):2328–2337. https://doi.org/10.1161/STROKEAHA.120.030696

66. Song T (2019) Generative model-based ischemic stroke lesion segmentation. https://doi.org/10.48550/arXiv.1906.02392

67. Clerigues A, Valverde S, Bernal J, Freixenet J, Oliver A, Llado X (2019) Acute ischemic stroke lesion core segmentation in CT perfusion images using fully convolutional neural networks. Comput Biol Med 115:103487. https://doi.org/10.1016/j.compbiomed.2019.103487

68. Mazdak Abulnaga S, Rubin J (2018) ischemic stroke lesion segmentation in CT perfusion scans using pyramid pooling and focal loss. https://doi.org/10.48550/arXiv.1811.01085

69. Lin T-Y, Dollár P, Girshick R, He K, Hariharan B, Belongie S (2016) Feature pyramid networks for object detection. https://doi.org/10.48550/arXiv.1612.03144

70. Winzeck S, Hakim A, McKinley R, Pinto J, Alves V, Silva C et al (2018) ISLES 2016 and 2017-benchmarking ischemic stroke lesion outcome prediction based on multispectral MRI. Front Neurol 9:679. https://doi.org/10.3389/fneur.2018.00679

71. Pinto A, McKinley R, Alves V, Wiest R, Silva CA, Reyes M (2018) Stroke lesion outcome prediction based on MRI imaging combined with clinical information. Front Neurol 9:1060. https://doi.org/10.3389/fneur.2018.01060

72. Cho K, van Merrienboer B, Gulcehre C, Bahdanau D, Bougares F, Schwenk H, et al. Learning phrase representations using RNN encoder-decoder for statistical machine translation. 2014

73. Nielsen A, Hansen MB, Tietze A, Mouridsen K (2018) Prediction of tissue outcome and assessment of treatment effect in acute ischemic stroke using deep learning. Stroke 49(6):1394–1401. https://doi.org/10.1161/STROKEAHA.117.019740

74. Ho KC, Scalzo F, Sarma KV, Speier W, El-Saden S, Arnold C (2019) Predicting ischemic stroke tissue fate using a deep convolutional neural network on source magnetic resonance perfusion images. J Med Imaging (Bellingham) 6(2):026001. https://doi.org/10.1117/1.JMI.6.2.026001

75. Yu Y, Xie Y, Thamm T, Gong E, Ouyang J, Huang C et al (2020) Use of deep learning to predict final ischemic stroke lesions from initial magnetic resonance imaging. JAMA Netw Open 3(3):e200772. https://doi.org/10.1001/jamanetworkopen.2020.0772

76. Yu Y, Xie Y, Thamm T, Gong E, Ouyang J, Christensen S et al (2021) Tissue at risk and ischemic core estimation using deep learning in acute stroke. AJNR Am J Neuroradiol. https://doi.org/10.3174/ajnr.A7081

77. Wang K, Shou Q, Ma SJ, Liebeskind D, Qiao XJ, Saver J et al (2020) Deep learning detection of penumbral tissue on arterial spin labeling in stroke. Stroke 51(2):489–497. https://doi.org/10.1161/STROKEAHA.119.027457

78. Robben D, Boers AMM, Marquering HA, Langezaal L, Roos Y, van Oostenbrugge RJ et al (2020) Prediction of final infarct volume from native CT perfusion and treatment parameters using deep learning. Med Image Anal 59:101589. https://doi.org/10.1016/j.media.2019.101589

79. Amador K, Wilms M, Winder A, Fiehler J, Forkert N (2021) Stroke lesion outcome prediction based on 4D CT perfusion data using temporal convolutional networks. In: Mattias H, Qi D, Marleen de B, Jan L, Alexander S, Floris E (eds) Proceedings of the fourth conference on medical imaging with deep learning. Proceedings of Machine Learning Research. PMLR, pp 22–33

80. Kuang H, Qiu W, Boers AM, Brown S, Muir K, Majoie C et al (2021) Computed tomography perfusion-based machine learning model better predicts follow-up infarction in patients with acute ischemic stroke. Stroke 52(1):223–231. https://doi.org/10.1161/STROKEAHA.120.030092

81. Yu Y, Parsi B, Speier W, Arnold C, Lou M, Scalzo F (2019) LSTM network for prediction of hemorrhagic transformation in acute stroke. Medical image computing and computer-assisted intervention. Springer, Cham, pp 177–185

82. Yu Y, Guo D, Lou M, Liebeskind D, Scalzo F (2018) Prediction of hemorrhagic transformation severity in acute stroke from source perfusion MRI. IEEE Trans Biomed Eng 65(9):2058–2065. https://doi.org/10.1109/TBME.2017.2783241

83. Jiang L, Zhou L, Yong W, Cui J, Geng W, Chen H et al (2021) A deep learning-based model for prediction of hemorrhagic transformation after stroke. Brain Pathol:e13023. https://doi.org/10.1111/bpa.13023

84. Nishi H, Oishi N, Ishii A, Ono I, Ogura T, Sunohara T et al (2019) Predicting clinical outcomes of large vessel occlusion before mechanical thrombectomy using machine learning. Stroke 50(9):2379–2388. https://doi.org/10.1161/STROKEAHA.119.025411

85. Heo J, Yoon JG, Park H, Kim YD, Nam HS, Heo JH (2019) Machine learning-based model for prediction of outcomes in acute stroke. Stroke 50(5):1263–1265. https://doi.org/10.1161/STROKEAHA.118.024293

86. Ntaios G, Faouzi M, Ferrari J, Lang W, Vemmos K, Michel P (2012) An integer-based score to predict functional outcome in acute ischemic stroke: the ASTRAL score. Neurology 78(24):1916–1922. https://doi.org/10.1212/WNL.0b013e318259e221

87. Ho KC, Speier W, El-Saden S, Liebeskind DS, Saver JL, Bui AA et al (2014) Predicting discharge mortality after acute ischemic stroke using balanced data. AMIA Annu Symp Proc 2014:1787–1796

88. van Os HJA, Ramos LA, Hilbert A, van Leeuwen M, van Walderveen MAA, Kruyt ND et al (2018) Predicting outcome of endovascular treatment for acute ischemic stroke: potential value of machine learning algorithms. Front Neurol 9:784. https://doi.org/10.3389/fneur.2018.00784

89. Xie Y, Jiang B, Gong E, Li Y, Zhu G, Michel P et al (2019) JOURNAL CLUB: use of gradient boosting machine learning to predict patient outcome in acute ischemic stroke on the basis of imaging, demographic, and clinical information. AJR Am J Roentgenol 212(1):44–51. https://doi.org/10.2214/AJR.18.20260

90. Osama S, Zafar K, Sadiq MU (2020) Predicting clinical outcome in acute ischemic stroke using parallel multi-parametric feature embedded Siamese network. Diagnostics (Basel) 10(11):858. https://doi.org/10.3390/diagnostics10110858

91. Chicco D (2021) Siamese neural networks: an overview. Methods Mol Biol 2190:73–94. https://doi.org/10.1007/978-1-0716-0826-5_3

92. Nishi H, Oishi N, Ishii A, Ono I, Ogura T, Sunohara T et al (2020) Deep learning-derived high-level neuroimaging features predict clinical outcomes for large vessel occlusion. Stroke 51(5):1484–1492. https://doi.org/10.1161/STROKEAHA.119.028101

93. Guo J, Gong E, Fan AP, Goubran M, Khalighi MM, Zaharchuk G (2020) Predicting (15)O-Water PET cerebral blood flow maps from multi-contrast MRI using a deep convolutional neural network with evaluation of training cohort bias. J Cereb Blood Flow Metab 40(11):2240–2253. https://doi.org/10.1177/0271678X19888123

94. Gupta A, Chazen JL, Hartman M, Delgado D, Anumula N, Shao H et al (2012) Cerebrovascular reserve and stroke risk in patients with carotid stenosis or occlusion: a systematic review and meta-analysis. Stroke 43(11):2884–2891. https://doi.org/10.1161/STROKEAHA.112.663716

95. Chen DYT, Ishii Y, Fan AP, Guo J, Zhao MY, Steinberg GK et al (2020) Predicting PET cerebrovascular reserve with deep learning by using baseline MRI: a pilot investigation of a drug-free brain stress test. Radiology 296(3):627–637. https://doi.org/10.1148/radiol.2020192793

96. Collaborators GBDS (2019) Global, regional, and national burden of stroke, 1990-2016: a systematic analysis for the global burden of disease study 2016. Lancet Neurol 18(5):439–458. https://doi.org/10.1016/S1474-4422(19)30034-1

97. Chilamkurthy S, Ghosh R, Tanamala S, Biviji M, Campeau NG, Venugopal VK et al (2018) Deep learning algorithms for detection of critical findings in head CT scans: a retrospective study. Lancet 392(10162):2388–2396. https://doi.org/10.1016/S0140-6736(18)31645-3

98. Lee H, Yune S, Mansouri M, Kim M, Tajmir SH, Guerrier CE et al (2019) An explainable deep-learning algorithm for the detection of acute intracranial haemorrhage from small datasets. Nat Biomed Eng 3(3):173–182. https://doi.org/10.1038/s41551-018-0324-9

99. Kuo W, Hne C, Mukherjee P, Malik J, Yuh EL (2019) Expert-level detection of acute

intracranial hemorrhage on head computed tomography using deep learning. Proc Natl Acad Sci U S A 116(45):22737–22745. https://doi.org/10.1073/pnas.1908021116

100. Zhang Y, Zhang B, Liang F, Liang S, Zhang Y, Yan P et al (2019) Radiomics features on non-contrast-enhanced CT scan can precisely classify AVM-related hematomas from other spontaneous intraparenchymal hematoma types. Eur Radiol 29(4):2157–2165. https://doi.org/10.1007/s00330-018-5747-x

101. Wang T, Lei Y, Tian S, Jiang X, Zhou J, Liu T et al (2019) Learning-based automatic segmentation of arteriovenous malformations on contrast CT images in brain stereotactic radiosurgery. Med Phys 46(7):3133–3141. https://doi.org/10.1002/mp.13560

102. Lee CC, Yang HC, Lin CJ, Chen CJ, Wu HM, Shiau CY et al (2019) Intervening nidal brain parenchyma and risk of radiation-induced changes after radiosurgery for brain arteriovenous malformation: a study using an unsupervised machine learning algorithm. World Neurosurg 125:e132–e1e8. https://doi.org/10.1016/j.wneu.2018.12.220

103. Turan N, Heider RA, Roy AK, Miller BA, Mullins ME, Barrow DL et al (2018) Current perspectives in imaging modalities for the assessment of unruptured intracranial aneurysms: a comparative analysis and review. World Neurosurg 113:280–292. https://doi.org/10.1016/j.wneu.2018.01.054

104. Yoon NK, McNally S, Taussky P, Park MS (2016) Imaging of cerebral aneurysms: a clinical perspective. Neurovasc Imaging 2(1):6. https://doi.org/10.1186/s40809-016-0016-3

105. Jaja BNR, Cusimano MD, Etminan N, Hanggi D, Hasan D, Ilodigwe D et al (2013) Clinical prediction models for aneurysmal subarachnoid hemorrhage: a systematic review. Neurocrit Care 18(1):143–153. https://doi.org/10.1007/s12028-012-9792-z

106. Hemphill JC, Greenberg SM, Anderson CS, Becker K, Bendok BR, Cushman M et al (2015) Guidelines for the management of spontaneous intracerebral hemorrhage: a guideline for healthcare professionals from the American Heart Association/American Stroke Association. Stroke 46(7):2032–2060. https://doi.org/10.1161/STR.0000000000000069

107. Ois A, Vivas E, Figueras-Aguirre G, Guimaraens L, Cuadrado-Godia E, Avellaneda C et al (2019) Misdiagnosis worsens prognosis in subarachnoid hemorrhage with good Hunt and Hess score. Stroke 50(11):3072–3076. https://doi.org/10.1161/STROKEAHA.119.025520

108. Lubicz B, Levivier M, François O, Thoma P, Sadeghi N, Collignon L et al (2007) Sixty-four-row multisection CT angiography for detection and evaluation of ruptured intracranial aneurysms: interobserver and intertechnique reproducibility. AJNR Am J Neuroradiol 28(10):1949–1955. https://doi.org/10.3174/ajnr.A0699

109. Okahara M, Kiyosue H, Yamashita M, Nagatomi H, Hata H, Saginoya T et al (2002) Diagnostic accuracy of magnetic resonance angiography for cerebral aneurysms in correlation with 3D-digital subtraction angiographic images: a study of 133 aneurysms. Stroke 33(7):1803–1808. https://doi.org/10.1161/01.str.0000019510.32145.a9

110. White PM, Teasdale EM, Wardlaw JM, Easton V (2001) Intracranial aneurysms: CT angiography and MR angiography for detection prospective blinded comparison in a large patient cohort. Radiology 219(3):739–749. https://doi.org/10.1148/radiology.219.3.r01ma16739

111. Yang X, Blezek DJ, Cheng LTE, Ryan WJ, Kallmes DF, Erickson BJ (2011) Computer-aided detection of intracranial aneurysms in MR angiography. J Digit Imaging 24(1):86–95. https://doi.org/10.1007/s10278-009-9254-0

112. Shi Z, Hu B, Schoepf UJ, Savage RH, Dargis DM, Pan CW et al (2020) Artificial intelligence in the management of intracranial aneurysms: current status and future perspectives. AJNR Am J Neuroradiol 41(3):373–379. https://doi.org/10.3174/ajnr.A6468

113. Nakao T, Hanaoka S, Nomura Y, Sato I, Nemoto M, Miki S et al (2018) Deep neural network-based computer-assisted detection of cerebral aneurysms in MR angiography. J Magn Reson Imaging 47(4):948–953. https://doi.org/10.1002/jmri.25842

114. Ueda D, Yamamoto A, Nishimori M, Shimono T, Doishita S, Shimazaki A et al (2019) Deep learning for MR angiography: automated detection of cerebral aneurysms. Radiology 290(1):187–194. https://doi.org/10.1148/radiol.2018180901

115. Park A, Chute C, Rajpurkar P, Lou J, Ball RL, Shpanskaya K et al (2019) Deep learning-assisted diagnosis of cerebral aneurysms using the HeadXNet model. JAMA Netw Open 2(6):e195600. https://doi.org/10.1001/jamanetworkopen.2019.5600

116. Dai X, Huang L, Qian Y, Xia S, Chong W, Liu J et al (2020) Deep learning for automated cerebral aneurysm detection on computed tomography images. Int J Comput Assist Radiol Surg 15(4):715–723. https://doi.org/10.1007/s11548-020-02121-2

117. Zeng Y, Liu X, Xiao N, Li Y, Jiang Y, Feng J et al (2019) Automatic diagnosis based on spatial information fusion feature for intracranial aneurysm. IEEE Trans Med Imaging. https://doi.org/10.1109/TMI.2019.2951439

118. Duan H, Huang Y, Liu L, Dai H, Chen L, Zhou L (2019) Automatic detection on intracranial aneurysm from digital subtraction angiography with cascade convolutional neural networks. Biomed Eng Online 18(1):110. https://doi.org/10.1186/s12938-019-0726-2

119. Sichtermann T, Faron A, Sijben R, Teichert N, Freiherr J, Wiesmann M (2019) Deep learning-based detection of intracranial aneurysms in 3D TOF-MRA. AJNR Am J Neuroradiol 40(1):25–32. https://doi.org/10.3174/ajnr.A5911

120. Faron A, Sichtermann T, Teichert N, Luetkens JA, Keulers A, Nikoubashman O et al (2019) Performance of a deep-learning neural network to detect intracranial aneurysms from 3D TOF-MRA compared to human readers. Clin Neuroradiol. https://doi.org/10.1007/s00062-019-00809-w

121. Investigators UJ, Morita A, Kirino T, Hashi K, Aoki N, Fukuhara S et al (2012) The natural course of unruptured cerebral aneurysms in a Japanese cohort. N Engl J Med 366(26):2474–2482. https://doi.org/10.1056/NEJMoa1113260

122. Naggara ON, Lecler A, Oppenheim C, Meder J-F, Raymond J (2012) Endovascular treatment of intracranial unruptured aneurysms: a systematic review of the literature on safety with emphasis on subgroup analyses. Radiology 263(3):828–835. https://doi.org/10.1148/radiol.12112114

123. Thompson BG, Brown RD, Amin-Hanjani S, Broderick JP, Cockroft KM, Connolly ES et al (2015) Guidelines for the management of patients with unruptured intracranial aneurysms: a guideline for healthcare professionals from the American Heart Association/American Stroke Association. Stroke 46(8):2368–2400. https://doi.org/10.1161/STR.0000000000000070

124. Wiebers DO, Whisnant JP, Huston J, Meissner I, Brown RD, Piepgras DG et al (2003) Unruptured intracranial aneurysms: natural history, clinical outcome, and risks of surgical and endovascular treatment. Lancet (London, England) 362(9378):103–110. https://doi.org/10.1016/s0140-6736(03)13860-3

125. Murayama Y, Fujimura S, Suzuki T, Takao H (2019) Computational fluid dynamics as a risk assessment tool for aneurysm rupture. Neurosurg Focus 47(1):E12. https://doi.org/10.3171/2019.4.FOCUS19189

126. Chien A, Sayre J (2014) Morphologic and hemodynamic risk factors in ruptured aneurysms imaged before and after rupture. AJNR Am J Neuroradiol 35(11):2130–2135. https://doi.org/10.3174/ajnr.A4016

127. Cornelissen BMW, Schneiders JJ, Potters WV, van den Berg R, Velthuis BK, Rinkel GJE et al (2015) Hemodynamic differences in intracranial aneurysms before and after rupture. AJNR Am J Neuroradiol 36(10):1927–1933. https://doi.org/10.3174/ajnr.A4385

128. Sugiyama S-I, Endo H, Omodaka S, Endo T, Niizuma K, Rashad S et al (2016) Daughter sac formation related to blood inflow jet in an intracranial aneurysm. World Neurosurg 96:396–402. https://doi.org/10.1016/j.wneu.2016.09.040

129. Stember JN, Chang P, Stember DM, Liu M, Grinband J, Filippi CG et al (2019) Convolutional neural networks for the detection and measurement of cerebral aneurysms on magnetic resonance angiography. J Digit Imaging 32(5):808–815. https://doi.org/10.1007/s10278-018-0162-z

130. Podgorsak AR, Rava RA, Shiraz Bhurwani MM, Chandra AR, Davies JM, Siddiqui AH et al (2019) Automatic radiomic feature extraction using deep learning for angiographic parametric imaging of intracranial aneurysms. J Neurointerv Surg. https://doi.org/10.1136/neurintsurg-2019-015214

131. Zhao X, Gold N, Fang Y, Xu S, Zhang Y, Liu J et al (2018) Vertebral artery fusiform aneurysm geometry in predicting rupture risk. R Soc Open Sci 5(10):180780. https://doi.org/10.1098/rsos.180780

132. Liu Q, Jiang P, Jiang Y, Ge H, Li S, Jin H et al (2019) Prediction of aneurysm stability using a machine learning model based on PyRadiomics-derived morphological features. Stroke 50(9):2314–2321. https://doi.org/10.1161/STROKEAHA.119.025777

133. Kim HC, Rhim JK, Ahn JH, Park JJ, Moon JU, Hong EP et al (2019) Machine learning application for rupture risk assessment in small-sized intracranial aneurysm. J Clin Med 8(5):683. https://doi.org/10.3390/jcm8050683

134. Paliwal N, Jaiswal P, Tutino VM, Shallwani H, Davies JM, Siddiqui AH et al (2018) Outcome prediction of intracranial aneurysm treatment by flow diverters using machine learning. Neurosurg Focus 45(5):E7. https://doi.org/10.3171/2018.8.FOCUS18332

135. Liu J, Chen Y, Lan L, Lin B, Chen W, Wang M et al (2018) Prediction of rupture risk in anterior communicating artery aneurysms with a feed-forward artificial neural network. Eur Radiol 28(8):3268–3275. https://doi.org/10.1007/s00330-017-5300-3

136. Varble N, Tutino VM, Yu J, Sonig A, Siddiqui AH, Davies JM et al (2018) Shared and distinct rupture discriminants of small and large intracranial aneurysms. Stroke 49(4):856–864. https://doi.org/10.1161/STROKEAHA.117.019929

137. Detmer FJ, Luckehe D, Mut F, Slawski M, Hirsch S, Bijlenga P et al (2019) Comparison of statistical learning approaches for cerebral aneurysm rupture assessment. Int J Comput Assist Radiol Surg. https://doi.org/10.1007/s11548-019-02065-2

138. Tanioka S, Ishida F, Yamamoto A, Shimizu S, Sakaida H, Toyoda M et al (2020) Machine learning classification of cerebral aneurysm rupture status with morphologic variables and hemodynamic parameters. Radiol Artif Intell 2(1):e190077. https://doi.org/10.1148/ryai.2019190077

139. Shi Z, Chen GZ, Mao L, Li XL, Zhou CS, Xia S et al (2021) Machine learning-based prediction of small intracranial aneurysm rupture status using CTA-derived hemodynamics: a multicenter study. AJNR Am J Neuroradiol 42(4):648–654. https://doi.org/10.3174/ajnr.A7034

140. Kim KH, Koo HW, Lee BJ, Sohn MJ (2021) Analysis of risk factors correlated with angiographic vasospasm in patients with aneurysmal subarachnoid hemorrhage using explainable predictive modeling. J Clin Neurosci 91:334–342. https://doi.org/10.1016/j.jocn.2021.07.028

141. Ramos LA, van der Steen WE, Sales Barros R, Majoie C, van den Berg R, Verbaan D et al (2019) Machine learning improves prediction of delayed cerebral ischemia in patients with subarachnoid hemorrhage. J Neurointerv Surg. 11(5):497–502. https://doi.org/10.1136/neurintsurg-2018-014258

142. Rubbert C, Patil KR, Beseoglu K, Mathys C, May R, Kaschner MG et al (2018) Prediction of outcome after aneurysmal subarachnoid haemorrhage using data from patient admission. Eur Radiol 28(12):4949–4958. https://doi.org/10.1007/s00330-018-5505-0

143. Wardlaw JM, Smith C, Dichgans M (2013) Mechanisms of sporadic cerebral small vessel disease: insights from neuroimaging. Lancet Neurol 12(5):483–497. https://doi.org/10.1016/S1474-4422(13)70060-7

144. Wardlaw JM, Smith EE, Biessels GJ, Cordonnier C, Fazekas F, Frayne R et al (2013) Neuroimaging standards for research into small vessel disease and its contribution to ageing and neurodegeneration. Lancet Neurol 12(8):822–838

145. Wardlaw JM, Smith C, Dichgans M (2019) Small vessel disease: mechanisms and clinical implications. Lancet Neurol 18(7):684–696. https://doi.org/10.1016/S1474-4422(19)30079-1

146. Debette S, Schilling S, Duperron M-G, Larsson SC, Markus HS (2019) Clinical significance of magnetic resonance imaging markers of vascular brain injury: a systematic review and meta-analysis. JAMA Neurol 76(1):81–94. https://doi.org/10.1001/jamaneurol.2018.3122

147. Kwon HM, Lynn MJ, Turan TN, Derdeyn CP, Fiorella D, Lane BF et al (2016) Frequency, risk factors, and outcome of coexistent small vessel disease and intracranial arterial stenosis: results from the Stenting and Aggressive Medical Management for Preventing Recurrent Stroke in Intracranial Stenosis (SAMMPRIS) Trial. JAMA Neurol 73(1):36–42. https://doi.org/10.1001/jamaneurol.2015.3145

148. Pasi M, Cordonnier C (2020) Clinical relevance of cerebral small vessel diseases. Stroke 51(1):47–53. https://doi.org/10.1161/STROKEAHA.119.024148

149. Kapasi A, DeCarli C, Schneider JA (2017) Impact of multiple pathologies on the threshold for clinically overt dementia. Acta Neuropathol 134(2):171–186. https://doi.org/10.1007/s00401-017-1717-7

150. Bos D, Wolters FJ, Darweesh SKL, Vernooij MW, Wolf F, Ikram MA et al (2018) Cerebral small vessel disease and the risk of dementia: a systematic review and meta-analysis of population-based evidence. Alzheimers Dement 14(11):1482–1492. https://doi.org/10.1016/j.jalz.2018.04.007

151. Akoudad S, Wolters FJ, Viswanathan A, Bruijn RF, Lugt A, Hofman A et al (2016) Association of cerebral microbleeds with cognitive decline and dementia. JAMA Neurol 73(8):934–943. https://doi.org/10.1001/jamaneurol.2016.1017

152. Brown R, Benveniste H, Black SE, Charpak S, Dichgans M, Joutel A et al (2018) Understanding the role of the perivascular space in cerebral small vessel disease. Cardiovasc Res 114(11):1462–1473. https://doi.org/10.1093/cvr/cvy113

153. Georgakis MK, Duering M, Wardlaw JM, Dichgans M (2019) WMH and long-term outcomes in ischemic stroke: a systematic review and meta-analysis. Neurology 92(12):e1298–ee308. https://doi.org/10.1212/WNL.0000000000007142

154. Staals J, Makin SD, Doubal FN, Dennis MS, Wardlaw JM (2014) Stroke subtype, vascular risk factors, and total MRI brain small-vessel disease burden. Neurology 83(14):1228–1234. https://doi.org/10.1212/WNL.0000000000000837

155. Xu X, Hilal S, Collinson SL, Chong EJY, Ikram MK, Venketasubramanian N et al (2015) Association of magnetic resonance imaging markers of cerebrovascular disease burden and cognition. Stroke 46(10):2808–2814. https://doi.org/10.1161/STROKEAHA.115.010700

156. Prins ND, Scheltens P (2015) White matter hyperintensities, cognitive impairment and dementia: an update. Nat Rev Neurol 11(3):157–165. https://doi.org/10.1038/nrneurol.2015.10

157. Fazekas F, Chawluk JB, Alavi A, Hurtig HI, Zimmerman RA (1987) MR signal abnormalities at 1.5 T in Alzheimer's dementia and normal aging. AJR Am J Roentgenol 149(2):351–356. https://doi.org/10.2214/ajr.149.2.351

158. Heuvel DMJ, Dam VH, Craen AJM, Admiraal-Behloul F, Es ACGM, Palm WM et al (2006) Measuring longitudinal white matter changes: comparison of a visual rating scale with a volumetric measurement. AJNR Am J Neuroradiol 27(4):875–878

159. Straaten ECW, Fazekas F, Rostrup E, Scheltens P, Schmidt R, Pantoni L et al (2006) Impact of white matter hyperintensities scoring method on correlations with clinical data: the LADIS study. Stroke 37(3):836–840. https://doi.org/10.1161/01.STR.0000202585.26325.74

160. Mäntylä R, Erkinjuntti T, Salonen O, Aronen HJ, Peltonen T, Pohjasvaara T et al (1997) Variable agreement between visual rating scales for white matter hyperintensities on MRI. Comparison of 13 rating scales in a poststroke cohort. Stroke 28(8):1614–1623. https://doi.org/10.1161/01.str.28.8.1614

161. Anbeek P, Vincken KL, Osch MJP, Bisschops RHC, Grond J (2004) Probabilistic segmentation of white matter lesions in MR imaging. NeuroImage 21(3):1037–1044. https://doi.org/10.1016/j.neuroimage.2003.10.012

162. Lao Z, Shen D, Liu D, Jawad AF, Melhem ER, Launer LJ et al (2008) Computer-assisted segmentation of white matter lesions in 3D MR images using support vector machine. Acad Radiol 15(3):300–313. https://doi.org/10.1016/j.acra.2007.10.012

163. Herskovits EH, Bryan RN, Yang F (2008) Automated Bayesian segmentation of micro-vascular white-matter lesions in the ACCORD-MIND study. Adv Med Sci 53(2):182–190. https://doi.org/10.2478/v10039-008-0039-3

164. Beare R, Srikanth V, Chen J, Phan TG, Stapleton J, Lipshut R et al (2009) Development and validation of morphological segmentation of age-related cerebral white matter hyperintensities. NeuroImage 47(1):199–203. https://doi.org/10.1016/j.neuroimage.2009.03.055

165. Dyrby TB, Rostrup E, Baaré WFC, Straaten ECW, Barkhof F, Vrenken H et al (2008) Segmentation of age-related white matter changes in a clinical multi-center study. NeuroImage 41(2):335–345. https://doi.org/10.1016/j.neuroimage.2008.02.024

166. Jack CR, O'Brien PC, Rettman DW, Shiung MM, Xu Y, Muthupillai R et al (2001) FLAIR histogram segmentation for measurement of leukoaraiosis volume. J Magn Reson Imaging 14(6):668–676. https://doi.org/10.1002/jmri.10011

167. Admiraal-Behloul F, Heuvel DMJ, Olofsen H, Osch MJP, Grond J, Buchem MA et al (2005) Fully automatic segmentation of white matter hyperintensities in MR images of the elderly. NeuroImage 28(3):607–617. https://doi.org/10.1016/j.neuroimage.2005.06.061

168. Seghier ML, Ramlackhansingh A, Crinion J, Leff AP, Price CJ (2008) Lesion identification using unified segmentation-normalisation models and fuzzy clustering. NeuroImage 41(4):1253–1266. https://doi.org/10.1016/j.neuroimage.2008.03.028

169. Wang Y, Catindig JA, Hilal S, Soon HW, Ting E, Wong TY et al (2012) Multi-stage segmentation of white matter hyperintensity, cortical and lacunar infarcts. NeuroImage 60(4):2379–2388. https://doi.org/10.1016/j.neuroimage.2012.02.034

170. Jeon S, Yoon U, Park J-S, Seo SW, Kim J-H, Kim ST et al (2011) Fully automated pipeline for quantification and localization of white

matter hyperintensity in brain magnetic resonance image. Int J Imaging Syst Technol 21(2):193–200. https://doi.org/10.1002/ima.20277

171. Caligiuri ME, Perrotta P, Augimeri A, Rocca F, Quattrone A, Cherubini A (2015) Automatic detection of white matter hyperintensities in healthy aging and pathology using magnetic resonance imaging: a review. Neuroinformatics 13(3):261–276. https://doi.org/10.1007/s12021-015-9260-y

172. Kuijf HJ, Biesbroek JM, De Bresser J, Heinen R, Andermatt S, Bento M et al (2019) Standardized assessment of automatic segmentation of white matter hyperintensities and results of the WMH segmentation challenge. IEEE Trans Med Imaging 38(11): 2556–2568. https://doi.org/10.1109/TMI.2019.2905770

173. Li H, Jiang G, Zhang J, Wang R, Wang Z, Zheng W-S et al (2018) Fully convolutional network ensembles for white matter hyperintensities segmentation in MR images. NeuroImage 183:650–665. https://doi.org/10.1016/j.neuroimage.2018.07.005

174. Andermatt S, Pezold S, Cattin P (2016) Multi-dimensional gated recurrent units for the segmentation of biomedical 3D-data. https://doi.org/10.1007/978-3-319-46976-8_15

175. Ghafoorian M, Karssemeijer N, Heskes T, Uden IWM, Sanchez CI, Litjens G et al (2017) Location sensitive deep convolutional neural networks for segmentation of white matter hyperintensities. Sci Rep 7(1):5110. https://doi.org/10.1038/s41598-017-05300-5

176. Valverde S, Cabezas M, Roura E, González-Villà S, Pareto D, Vilanova JC et al (2017) Improving automated multiple sclerosis lesion segmentation with a cascaded 3D convolutional neural network approach. NeuroImage 155:159–168. https://doi.org/10.1016/j.neuroimage.2017.04.034

177. Zhang Z, Powell K, Yin C, Cao S, Gonzalez D, Hannawi Y et al (2021) Brain atlas guided attention U-net for white matter hyperintensity segmentation. AMIA Jt Summits Transl Sci Proc 2021:663–671

178. Park G, Hong J, Duffy BA, Lee J-M, Kim H (2021) White matter hyperintensities segmentation using the ensemble U-net with multi-scale highlighting foregrounds. NeuroImage 237:118140. https://doi.org/10.1016/j.neuroimage.2021.118140

179. Balakrishnan R, Valdés Hernández MC, Farrall AJ (2021) Automatic segmentation of white matter hyperintensities from brain magnetic resonance images in the era of deep learning and big data – a systematic review. Comput Med Imaging Graph 88: 101867. https://doi.org/10.1016/j.compmedimag.2021.101867

180. Jiang J, Liu T, Zhu W, Koncz R, Liu H, Lee T et al (2018) UBO detector – a cluster-based, fully automated pipeline for extracting white matter hyperintensities. NeuroImage 174: 539–549. https://doi.org/10.1016/j.neuroimage.2018.03.050

181. Sundaresan V, Zamboni G, Le Heron C, Rothwell PM, Husain M, Battaglini M et al (2019) Automated lesion segmentation with BIANCA: impact of population-level features, classification algorithm and locally adaptive thresholding. NeuroImage 202:116056. https://doi.org/10.1016/j.neuroimage.2019.116056

182. Zhan T, Yu R, Zheng Y, Zhan Y, Xiao L, Wei Z (2017) Multimodal spatial-based segmentation framework for white matter lesions in multi-sequence magnetic resonance images. Biomed Signal Process Control 31:52–62. https://doi.org/10.1016/j.bspc.2016.06.016

183. Ding T, Cohen AD, O'Connor EE, Karim HT, Crainiceanu A, Muschelli J et al (2020) An improved algorithm of white matter hyperintensity detection in elderly adults. Neuroimage Clin 25:102151. https://doi.org/10.1016/j.nicl.2019.102151

184. Zhan T, Zhan Y, Liu Z, Xiao L, Wei Z (2015) Automatic method for white matter lesion segmentation based on T1-fluid-attenuated inversion recovery images. IET Comput Vis 9(4):447–455. https://doi.org/10.1049/iet-cvi.2014.0121

185. Valverde S, Oliver A, Roura E, González-Villà S, Pareto D, Vilanova JC et al (2017) Automated tissue segmentation of MR brain images in the presence of white matter lesions. Med Image Anal 35:446–457. https://doi.org/10.1016/j.media.2016.08.014

186. Fiford CM, Sudre CH, Pemberton H, Walsh P, Manning E, Malone IB et al (2020) Automated White matter hyperintensity segmentation using Bayesian model selection: assessment and correlations with cognitive change. Neuroinformatics 18(3):429–449. https://doi.org/10.1007/s12021-019-09439-6

187. Damangir S, Westman E, Simmons A, Vrenken H, Wahlund L-O, Spulber G (2017) Reproducible segmentation of white matter hyperintensities using a new statistical definition. MAGMA 30(3):227–237.

https://doi.org/10.1007/s10334-016-0599-3

188. Vanderbecq Q, Xu E, Stroer S, Couvy-Duchesne B, Diaz Melo M, Dormont D et al (2020) Comparison and validation of seven white matter hyperintensities segmentation software in elderly patients. Neuroimage Clin 27:102357. https://doi.org/10.1016/j.nicl.2020.102357

189. Greenberg SM, Vernooij MW, Cordonnier C, Viswanathan A, Al-Shahi Salman R, Warach S et al (2009) Cerebral microbleeds: a guide to detection and interpretation. Lancet Neurol 8(2):165–174. https://doi.org/10.1016/S1474-4422(09)70013-4

190. Charidimou A, Shoamanesh A, Wilson D, Gang Q, Fox Z, Jager HR et al (2015) Cerebral microbleeds and postthrombolysis intracerebral hemorrhage risk updated meta-analysis. Neurology 85(11):927–924. https://doi.org/10.1212/WNL.0000000000001923

191. Wilson D, Ambler G, Shakeshaft C, Brown MM, Charidimou A, Al-Shahi Salman R et al (2018) Cerebral microbleeds and intracranial haemorrhage risk in patients anticoagulated for atrial fibrillation after acute ischaemic stroke or transient ischaemic attack (CROMIS-2): a multicentre observational cohort study. Lancet Neurol 17(6):539–547. https://doi.org/10.1016/S1474-4422(18)30145-5

192. Fazekas F, Kleinert R, Roob G, Kleinert G, Kapeller P, Schmidt R et al (1999) Histopathologic analysis of foci of signal loss on gradient-echo T2*-weighted MR images in patients with spontaneous intracerebral hemorrhage: evidence of microangiopathy-related microbleeds. AJNR Am J Neuroradiol 20(4):637–642

193. Knudsen KA, Rosand J, Karluk D, Greenberg SM (2001) Clinical diagnosis of cerebral amyloid angiopathy: validation of the Boston criteria. Neurology 56(4):537–539. https://doi.org/10.1212/wnl.56.4.537

194. van den Heuvel TL, van der Eerden AW, Manniesing R, Ghafoorian M, Tan T, Andriessen TM et al (2016) Automated detection of cerebral microbleeds in patients with traumatic brain injury. Neuroimage Clin 12:241–251. https://doi.org/10.1016/j.nicl.2016.07.002

195. Wang S, Tang C, Sun J, Zhang Y (2019) Cerebral micro-bleeding detection based on densely connected neural network. Front Neurosci 13:422. https://doi.org/10.3389/fnins.2019.00422

196. Liu S, Utriainen D, Chai C, Chen Y, Wang L, Sethi SK et al (2019) Cerebral microbleed detection using susceptibility weighted imaging and deep learning. NeuroImage 198:271–282. https://doi.org/10.1016/j.neuroimage.2019.05.046

197. Rashid T, Abdulkadir A, Nasrallah IM, Ware JB, Spincemaille P, Romero JR et al (2021) DEEPMIR: a DEEP convolutional neural network for differential detection of cerebral microbleeds and iron deposits in MRI. Sci Rep 11(1):14124

198. Dou Q, Chen H, Yu L, Zhao L, Qin J, Wang D et al (2016) Automatic detection of cerebral microbleeds from MR images via 3D convolutional neural networks. IEEE Trans Med Imaging 35(5):1182–1195. https://doi.org/10.1109/TMI.2016.2528129

199. Loos CMJ, Makin SDJ, Staals J, Dennis MS, Oostenbrugge RJ, Wardlaw JM (2018) Long-term morphological changes of symptomatic lacunar infarcts and surrounding White matter on structural magnetic resonance imaging. Stroke 49(5):1183–1188. https://doi.org/10.1161/STROKEAHA.117.020495

200. Duering M, Csanadi E, Gesierich B, Jouvent E, Hervé D, Seiler S et al (2013) Incident lacunes preferentially localize to the edge of white matter hyperintensities: insights into the pathophysiology of cerebral small vessel disease. Brain J Neurol 136(Pt 9):2717–2726. https://doi.org/10.1093/brain/awt184

201. Uchiyama Y, Asano T, Kato H, Hara T, Kanematsu M, Hoshi H et al (2012) Computer-aided diagnosis for detection of lacunar infarcts on MR images: ROC analysis of radiologists' performance. J Digit Imaging 25(4):497–503. https://doi.org/10.1007/s10278-011-9444-4

202. Ghafoorian M, Karssemeijer N, Heskes T, Bergkamp M, Wissink J, Obels J et al (2017) Deep multi-scale location-aware 3D convolutional neural networks for automated detection of lacunes of presumed vascular origin. Neuroimage Clin 14:391–399. https://doi.org/10.1016/j.nicl.2017.01.033

203. Jessen NA, Munk ASF, Lundgaard I, Nedergaard M (2015) The glymphatic system – a Beginner's guide. Neurochem Res 40(12):2583–2599. https://doi.org/10.1007/s11064-015-1581-6

204. Ding J, Sigurðsson S, Jónsson PV, Eiriksdottir G, Charidimou A, Lopez OL et al (2017) Large perivascular spaces visible on magnetic resonance imaging, cerebral small vessel disease progression, and risk of

dementia: the age, gene/environment susceptibility-Reykjavik study. JAMA Neurol 74(9):1105–1112. https://doi.org/10.1001/jamaneurol.2017.1397

205. Charidimou A, Martinez-Ramirez S, Reijmer YD, Oliveira-Filho J, Lauer A, Roongpiboonsopit D et al (2016) Total magnetic resonance imaging burden of small vessel disease in cerebral amyloid angiopathy: an imaging-pathologic study of concept validation. JAMA Neurol 73(8):994–1001. https://doi.org/10.1001/jamaneurol.2016.0832

206. Park SH, Zong X, Gao Y, Lin W, Shen D (2016) Segmentation of perivascular spaces in 7T MR image using auto-context model with orientation-normalized features. NeuroImage 134:223–235. https://doi.org/10.1016/j.neuroimage.2016.03.076

207. Ballerini L, Lovreglio R, Valdés Hernández MDC, Ramirez J, MacIntosh BJ, Black SE et al (2018) Perivascular spaces segmentation in brain MRI using optimal 3D filtering. Sci Rep 8(1):2132. https://doi.org/10.1038/s41598-018-19781-5

208. Dubost F, Yilmaz P, Adams H, Bortsova G, Ikram MA, Niessen W et al (2019) Enlarged perivascular spaces in brain MRI: automated quantification in four regions. NeuroImage 185:534–544. https://doi.org/10.1016/j.neuroimage.2018.10.026

209. Shi Y, Wardlaw JM (2016) Update on cerebral small vessel disease: a dynamic whole-brain disease. Stroke Vasc Neurol 1(3):83–92. https://doi.org/10.1136/svn-2016-000035

210. Biesbroek JM, Weaver NA, Biessels GJ (2017) Lesion location and cognitive impact of cerebral small vessel disease. Clin Sci (Lond) 131(8):715–728. https://doi.org/10.1042/CS20160452

211. Duan Y, Shan W, Liu L, Wang Q, Wu Z, Liu P et al (2020) Primary categorizing and masking cerebral small vessel disease based on "deep learning system". Front Neuroinform 14:17

212. Dickie DA, Valdés Hernández MDC, Makin SD, Staals J, Wiseman SJ, Bastin ME et al (2018) The brain health index: towards a combined measure of neurovascular and neurodegenerative structural brain injury. Int J Stroke 13(8):849–856. https://doi.org/10.1177/1747493018770222

213. Jokinen H, Koikkalainen J, Laakso HM, Melkas S, Nieminen T, Brander A et al (2020) Global burden of small vessel disease-related brain changes on MRI predicts cognitive and functional decline. Stroke 51(1):170–178. https://doi.org/10.1161/STROKEAHA.119.026170